# Listeriolysin O promotes the intravacuolar growth of Listeria monocytogenes in epithelial cells

Caroline Peron Cane, Julien Leblanc, Laure Wingertsmann, José Carlos Fernandez, Arnaud Gautier, Nicolas Desprat, Alice Lebreton



# Listeriolysin O promotes the intravacuolar growth of *Listeria monocytogenes* in epithelial cells

Caroline Peron Cane[1,2], Julien Leblanc[2], Laure Wingertsmann[2], José Carlos Fernandez[2], Arnaud Gautier[3,4], Nicolas Desprat[1,2,5‡] and Alice Lebreton[2,6‡]

[1] Laboratoire de Physique de l'École normale supérieure, ENS, PSL University, CNRS, Sorbonne Université, Université Paris Diderot, Sorbonne Paris-Cité, 75005 Paris, France.

[2] Institut de biologie de l'ENS (IBENS), Département de biologie, École normale supérieure, CNRS, INSERM, PSL University, 75005 Paris, France.

[3] Sorbonne Université, École normale supérieure, PSL University, CNRS, Laboratoire des Biomolécules, LBM, 75005 Paris, France.

[4] Institut Universitaire de France.

[5] UFR de Physique, Université Paris-Diderot, Université de Paris, 75005 Paris, France.

[6] INRAE, IBENS, 75005 Paris, France.

‡ Correspondence to: alice.lebreton@ens.fr; nicolas.desprat@phys.ens.fr

## Abstract

Upon entry into host cells, *Listeria monocytogenes* (*Lm*) was described to escape rapidly from internalisation vacuoles and proliferate only after gaining access to the cytosol. Vacuole escape depends upon three secreted virulence factors: the pore-forming toxin listeriolysin O (LLO) and two phospholipases. To quantify the dynamics of vacuolar escape, we used FAST fluorescent tags to monitor bacterial secretion into enclosed compartments. By tracking fluorescently-labelled vacuoles, we quantified the heterogeneity of *Lm* residence time in primary vacuoles formed in epithelial LoVo cells. Although half of the bacterial population escaped from vacuoles within 13 minutes after internalisation, a fraction of it remained entrapped several hours in Long Residence Vacuoles (LRV), for both wild type and LLO-deficient strains. Unexpectedly, *Lm* replicated inside LRVs at a rate similar to that in the cytosol. LRVs were decorated with LLO-FAST and LLO was necessary for bacterial proliferation in these compartments, suggesting that permeation of vacuolar membranes sustained growth. LRVs displayed similarities with the spacious *Listeria*-containing phagosomes described in macrophages, and could constitute an alternative replication niche for *Lm* in epithelial cells.

# Introduction

Bacterial pathogens harness distinct strategies to colonize their host and take advantage of its resources, for instance by adopting an intracellular lifestyle. Internalisation into host cells can allow invasive bacteria to cross the organism barriers, escape humoral immune surveillance, or disseminate throughout the organism as cargo of circulating cells. After internalisation, bacteria are entrapped inside primary vacuoles from where they can follow two distinct routes: either subverting endomembrane compartments, or leaving them. For instance, *Mycobacterium tuberculosis*, *Chlamydia trachomatis*, *Brucella abortus*, *Coxiella burnetii*, *Legionella pneumophila* perturb the maturation and rearrange the properties of vacuoles, thereby creating a compartment prone to their replication (reviewed in Salcedo & Holden, 2005; Di Russo Case & Samuel, 2016). Others, such as *Shigella flexneri* or *Listeria monocytogenes*, typically do not grow inside endomembrane compartments, but rather escape from entry vacuoles and gain access to the host cell cytoplasm, where they can replicate as well as exploit the host actin cytoskeleton for intracellular motility and cell-to-cell spread (reviewed in Gouin *et al*, 2005).

The foodborne pathogen *Listeria monocytogenes* (hereafter, *Lm*) is the causative agent of listeriosis, and has emerged as a model facultative intracellular bacterium (reviewed in Cossart & Lebreton, 2014; Radoshevich *et al*, 2015). This pathogen can cross the protective barriers of its host and colonize tissues and organs by promoting its internalisation into non-phagocytic cells. The classical scheme of *Lm* intracellular life cycle implies that, both in professional phagocytes and in epithelial cells, *Lm* rapidly escapes from entry vacuoles due to the combined action of a potent pore-forming toxin, listeriolysin O (LLO), and of two phospholipases C (PlcA and PlcB), before replicating in the cytosol (Pizarro-Cerda & Cossart, 2018). All three genes (*hlyA* that encodes LLO, *plcA* and *plcB*) are part of *Lm* LIPI-I virulence gene cluster and are transcriptionally induced by PrfA, the main regulator of *Lm* virulence gene, in intracellular bacteria (reviewed in las Heras *et al*, 2011; Lebreton & Cossart, 2017).

LLO is a cholesterol-dependent pore-forming toxin (reviewed in Nguyen *et al*, 2018), secreted by *Lm* via the general secretion system (Sec). LLO assembles into oligomers on biological membranes, forming arcs and pores of several tens of nm that disrupt membrane integrity (Köster *et al*, 2014; Ruan *et al*, 2016). Its activity is optimal at acidic pH representative of the acidification occurring during the maturation of phagosomes (pH = 4.9 to 6.7) (Beauregard *et al*, 1997; Schuerch *et al*, 2005), which has been proposed to facilitate the escape of bacteria from entry vacuoles while avoiding damages to the host plasma membranes at neutral pH. Whereas LLO-deficient *Lm* cannot gain access to the host cytosol in many cell types, the activity of the phospholipases PlcA and PlcB and the influence of host factors render LLO dispensable for vacuolar escape in several human epithelial cell lines (Marquis *et al*, 1995; Burrack *et al*, 2009). In phagocytes, it has been shown that bacteria secreting reduced amounts of LLO could remain entrapped in long-term compartments named Spacious *Listeria*-containing Phagosomes (SLAPs) and even replicate slowly therein, with a doubling time in the range of 8 h (Birmingham *et al*, 2008).

The escape dynamics from the entry vacuole has been experimentally addressed using several distinct strategies. One of them consisted in using medium containing a membrane-impermeant fluorescent dye during infection (Beauregard *et al*, 1997; Myers *et al*, 2003). Upon encapsulation in the primary entry vacuoles together with invading bacteria, the fluorescent dye stained the vacuolar space until it broke down. Alternative strategies were based on the assessment of vacuole rupture events and bacterial access to the host cytosol using fluorescent sensors. For instance, galectin-3 has been shown to label membrane remnants of damaged vacuoles and thereby allow the spotting of vacuole lysis (Paz *et al*, 2010). Likewise, actin or the Cell-wall Binding Domain CBD (a domain from the *Lm* phage endolysin Ply118) are recruited to the bacterial surface only once *Lm* has escaped the vacuole (Pizarro-Cerda & Cossart, 2018; Henry *et al*, 2006). Cytoplasmic FRET probes that are cleaved by a β-lactamase secreted by invasive bacteria have also been shown to be efficient reporters of vacuole rupture (Ray *et al*, 2010; Quereda *et al*, 2015). Even though these techniques yielded the order of magnitude of the time lapse between bacterial entry and vacuole escape in various cell types (between 15 min and 1 h), none of these tools has been used so far to determine the distribution of *Lm* residence time in entry vacuoles, which is limiting the interpretation of variations found between conditions.

In order to measure the heterogeneity of *Lm* residence time in entry vacuoles and to assess the role played by LLO in the dynamics of bacterial escape from these compartments, we developed live imaging assays allowing an accurate measurement of the time elapsed between the moment when individual bacteria are internalised into cells, and the moment when the vacuole membrane is ruptured. We devised a strategy relying on the tagging of proteins secreted by bacteria with the FAST reporter system (Plamont *et al*, 2016). FAST is a 14-kDa protein tag which displays fluorescence upon binding with a synthetic fluorogenic probe supplied in the medium. The fluorogen is membrane permeant, non-toxic, and has very little fluorescence by itself. The small size of FAST, its fast folding kinetics, the reversible binding of fluorogens together with good brightness and photostability make this system an ideal candidate for tagging secreted proteins and imaging them in real time.

Using live imaging of FAST, we quantified the distribution of *Lm* residence times in primary vacuoles in the LoVo intestinal epithelial cell line. We observed that a fraction of the population of entry vacuoles could last for several hours and are reminiscent of SLAPs. However, in contrast with SLAPs, these Long Residence Vacuoles (LRVs) were obtained in cells infected with wild type (WT) *Lm* as well as with a *hlyA* deletion strain. Furthermore, secretion of LLO inside LRVs allowed *Lm* to proliferate efficiently in these compartments, suggesting that besides its role in vacuolar escape, LLO could contribute to set up an intravacuolar niche prone to *Lm* replication in epithelial cells.

# Results

## FAST-tagging of secreted bacterial effectors for live microscopy

With the aim of detecting proteins that would be secreted by intracellular bacteria into their host cells in live-cell microscopy experiments, we explored the possibilities offered by the FAST reporter system for the fluorescent tagging of *Lm* secreted bacterial effectors. In order to investigate the ability of *Lm* to secrete FAST-tagged proteins via the Sec pathway, a set of integrative plasmids harbouring gene fusions under control of the $P_{HYPER}$ promoter were designed (Fig EV1A, Appendix Fig S1A). These plasmids drove the constitutive production of either FAST or eGFP, either for intrabacterial localisation, or fused in their N-terminus to the secretion signal peptide (SP) of listeriolysin O (LLO) (SP-FAST and SP-eGFP constructs), or to full-length LLO (LLO-FAST, LLO-eGFP and untagged LLO constructs), a classical Sec substrate. All constructs additionally encompassed a Myc tag in their C-terminus in order to allow detection by immunoblotting. Protein production and secretion by each one of these seven strains was assessed by colloidal Coomassie staining and immunoblotting against the Myc tag, on bacterial total extracts and culture supernatant fractions from overnight-grown cultures in BHI, separated by SDS-PAGE (Fig EV2). All transgenes were efficiently expressed by *Lm* strain LL195, even though in varying amounts. As expected, constructs harbouring either the LLO SP, or full-length LLO, were recovered in bacterial culture supernatants, suggesting that the SP of LLO promoted Sec-dependent export of FAST or FAST-tagged proteins, as well as eGFP-fusion proteins albeit to a lesser extent (Fig EV2C, D). Constructs devoid of signal peptides were not detected in supernatant fractions, arguing against the release of proteins into the medium due to bacterial lysis. FAST-tagged Sec substrates can thus efficiently undergo secretion trough the general secretion pathway.

To assess whether the FAST reporter system remained fluorescent after secretion, we quantified the fluorescence signals in the supernatants of bacterial cultures grown overnight in iLSM (Fig 1A). In presence of 5 µM of HBR-3,5-DM, fluorescence was detected in the supernatants of strains secreting SP-FAST or LLO-FAST. Fluorescence intensities in the culture medium of strains producing non-secreted FAST or eGFP did not significantly differ from that of the strain producing untagged LLO, indicating that the release of fluorescent proteins in the culture medium was not due to bacterial lysis, and that FAST-labelled proteins retain their fluorescent properties after undergoing secretion trough the bacterial Sec system. By calibrating fluorescence measurements with a standard curve of known FAST:HBR-3,5-DM concentrations diluted in the same minimal medium, we estimated the secreted concentration of tagged proteins. The concentration of secreted SP-FAST after an overnight culture was 325±55 nM, and that of LLO-FAST around 28±6 nM.

Several attempts by others with various Gram–negative or –positive bacteria (Dammeyer & Tinnefeld, 2012; van der Ploeg *et al*, 2012), and our own unpublished observations using tagged *Lm* virulence factors, indicated that the Sec-dependent secretion and subsequent maturation of an eGFP tag into its active, fluorescent fold was inefficient. Surprisingly, the secretion of SP-eGFP—but not that of LLO-eGFP—gave

rise to fluorescent signals in culture supernatants, even though in a range 10 fold lower than that obtained for the secretion of SP-FAST. A consistent proportion of eGFP undergoing Sec-dependent secretion is thus able to acquire its mature fold in bacterial culture medium, at least in iLSM, and when not fused to a bacterial effector.

To evaluate the versatility of FAST as a reporter of bacterial secretion, we next asked if FAST was suitable for fluorescent tagging of effectors secreted through the syringe of the type III secretion system (T3SS) from a Gram-negative pathogen, *Shigella flexneri* (*Sf*) strain M90T. As model substrates, we tagged C-terminally with FAST-Myc the effectors OspF and IpaB (Fig EV1B), which are translocated upon adhesion of *Sf* to host cells (reviewed in Pinaud *et al*, 2018). Bacterial total extracts and culture supernatant fractions were recovered from overnight-grown cultures in M9 medium, with or without stimulation of type-III dependent secretion by addition of Congo red. By immunoblotting these fractions against the Myc-tag, we observed that tagged OspF and IpaB were secreted into the bacterial culture medium upon Congo red induction (Fig EV3A). Constitutive secretion of both tagged effectors was observed when using a Δ*ipaD* mutant strain for which translocation lacks gating controls (Ménard *et al*, 1994) (Fig EV3B). We then assessed whether the fusion proteins secreted by the Δ*ipaD* strain had retained their fluorescent properties, by measuring fluorescence intensities in the supernatants of bacterial cultures grown overnight in M9 medium (Fig 1B). Fluorescence levels were consistently higher with this constitutively secreting strain than the fluorescence leakage measured for the WT strain when the T3SS was not induced. The concentration of OspF-FAST by the Δ*ipaD* strain was estimated to be 3.8 ± 0.3 nM, that of IpaB-FAST of 9.4 ± 1.7 nM. Like Sec substrates, FAST-tagged T3SS substrates can thus be translocated and keep fluorescent properties after secretion.

We then investigated whether the FAST reporter system was suited for intracellular detection in real-time microscopy of proteins secreted during infection. We monitored FAST signals in LoVo cells infected with *Lm* producing SP-FAST by confocal spinning disk microscopy over an infection time course (Fig 2, Movie EV1). FAST fluorescence increased uniformly over time in the cytoplasm of infected cells (Fig 2A). At 562 nm—the wavelength specific for FAST:HBR-3,5-DM—, fluorescent signals accumulated in cells infected with a strain producing SP-FAST, and not in a control isogenic strain that constitutively expressed mCherry (Fig 2B). In infected cells, fluorescence intensity—which corresponds to intracellular concentration of SP-FAST—increased exponentially over time (Fig 2C), likely mirroring the exponential growth of *Lm* in the host cytosol. After an exponential increase, the intracellular fluorescence dropped suddenly, corresponding to the death of infected cells and the permeation of their membranes. The distribution of exponential fluorescence increase rates in FAST fluorescence was indicative of the variability in the infection rates among infected cells (Fig 2D). The median rate was 0.66 $h^{-1}$, corresponding to a doubling time of 63 min. Consistently, a median bacterial growth rate of 0.72 $h^{-1}$ (doubling time of 58 min) was measured in similar conditions of infection and illumination by segmenting mCherry-labelled bacteria, and then measuring intrabacterial mCherry signals over time. The long tail of the distribution of exponential

fluorescence increase rates likely reflected additional entries due to cell-to-cell spread from neighbouring cells. Altogether, the secretion of FAST into host cells allowed a quantitative monitoring of infection progression by live imaging of individual cells.

## Residence time of *Listeria monocytogenes* in internalisation vacuoles

When FAST-tagged proteins were secreted into the large volume of the host cell cytoplasm, fluorescent signals were diluted and therefore only became visible after several hours of infection, once they had accumulated sufficiently enough to be significantly discriminated from non-specific signals. Meanwhile, we reasoned that if *Lm* was confined in micron-sized internalisation vacuoles, the higher concentration of secreted FAST molecules in a reduced volume could allow their detection and tracking until the rupture of vacuole membranes, thereby providing an accurate measurement of the lifetime of primary vacuoles (Fig 3A). Indeed, we observed that SP-FAST signals were enhanced in micro-sized compartments that co-localized with mCherry-expressing bacteria within minutes after bacterial adhesion to cells, until these signals suddenly dropped when vacuoles ruptured (Fig 3B, Movies EV2, EV3).

We used SP-FAST secretion to track intravacuolar fluorescent signals, and compare the residence time of WT or Δ*hlyA Lm* strains inside primary vacuoles formed in LoVo cells (Fig 3D-E). The *hlyA* deletion strain used in this experiment was generated by in-frame allelic replacement of the *hlyA* open reading frame with SP-FAST (Δ*hlyA*::SP-FAST, Fig EV1C). The median value for the residence time of the WT strain was of 12.7±0.7 min (Fig 3E). When using the Δ*hlyA*::SP-FAST strain, the median residence time was significantly longer (21.1 ± 1.4 min) but remained of the same order of magnitude as for a strain producing LLO, confirming previous observations that *Lm* gained efficient access to the cytoplasm independently of LLO in epithelial cells (Marquis *et al*, 1995; Burrack *et al*, 2009). Unexpectedly, a large proportion of the entry vacuoles lasted for more than one hour (12.0 % for the WT strain; 14.8 % for the Δ*hlyA* mutant), and a number of intact vacuoles were still observed 3 h p.i. (4.6 % for the WT strain; 6.2 % for the Δ*hlyA* mutant) (Fig 3D). The fact that the WT strain remained entrapped in Long Residence Vacuoles (LRVs) in nearly identical proportions as the Δ*hlyA* strain could either suggest that a sub-population of WT *Lm* failed to escape primary vacuoles in spite of LLO secretion, or that LLO was not produced in this sub-population of intravacuolar bacteria. To discriminate between these two hypotheses, we investigated whether LLO fused to a FAST tag was detected in vacuoles out of which *Lm* had failed to escape.

## Role of LLO for the long-term vacuolar residence and intravacuolar replication of *Listeria*

To examine whether LLO was produced and secreted by bacteria that remained entrapped in LRVs, we engineered a *Lm* strain where LLO was C-terminally fused with FAST at the endogenous *hlyA* locus (Fig EV1C). In this strain, the fluorescence of FAST reported not only for LLO secretion and localisation, but also for *hlyA* expression under its natural promoter. In order to be relevant for monitoring the dynamics of *Lm* intracellular infection, the 15kDa FAST-Myc tag should not interfere with the function of the protein it

reports for. We thus assessed the haemolytic properties of the strain expressing *hlyA-FAST*, which did not differ from that of the WT strain (Appendix Fig S2). The production, secretion and activity as a cytolysin of LLO are thus quantitatively and qualitatively preserved after C-terminal fusion with FAST.

The strain producing the LLO-FAST fusion was also constitutively expressing mCherry, which allowed us to segment and track bacteria in 3D during infection. When imaging mCherry-labelled bacteria and LLO-FAST from 2 h post-infection (p.i.) in LoVo cells, we observed that *Lm* could remained entrapped inside LRVs for 9 h before the rounded structure of LLO-labelled membranes eventually disrupted and bacteria dispersed into the cytosol (Fig 4A, Movie EV4). Strikingly, the volume occupied by the mCherry signal increased with time, revealing that not only *Lm* inhabited LRVs for a long time, but that it was multiplying inside these compartments. The ability of *Lm* to grow inside LLO-FAST-labelled vacuoles was observed for both the LL195 genetic background (*Lm* lineage I, ST1) and the European *Lm* reference strain EGD-e (lineage II, ST9) (Fig EV4A, Movie EV5), indicating that this property was not specific to the hypervirulent clone LL195. Likewise, the proliferation of *Lm* inside LRVs was observed in Caco-2 cells, suggesting that LoVo cells were not the only epithelial niche allowing *Lm* to replicate inside endomembrane compartments (Fig. EV4B).

By tracking growing vacuole and measuring their volume over time, we determined the growth rate of *Lm* inside long-lived vacuoles. *Lm* grew exponentially in LRVs, with a rate similar to that of free bacteria in the cytosol (Fig 4B, Fig EV5A). The observed doubling time (90 min in this experimental setup; or down to 1h when the intensity and frequency of illumination were reduced as in Fig. 2D) was consistently shorter than that previously described in SLAPS, which was in the range of 8 h (Birmingham *et al*, 2008).

Our observations suggested that even when LRVs were permeated by LLO, their integrity was maintained and they allowed intravacuolar replication without rupturing. To further investigate whether LLO influenced *Lm* residence in LRVs, we took advantage of the LLO-FAST reporter strain to assess the variability in LLO abundance in these compartments. LLO-FAST signals measured in LRVs were greater than background levels but displayed a broad range of dynamics, indicating that LRV formation and maintenance was independent of the amounts of secreted LLO (Fig EV5B). In some LRVs, LLO-FAST accumulated linearly over time, while others displayed large-scale fluctuations in the signal. Some LRVs yielded a strong signal while others displayed low levels of decoration by LLO. The lifetime of LRV was correlated with neither the average concentration of LLO (Appendix Fig S3A) nor its maximal level (Appendix Fig S3B), suggesting that LLO concentration poorly influenced the probability of *Lm* escape from these structures. Consistently, we observed that not only WT and Δ*hlyA Lm* could reside in long-term vacuoles (Fig 3D, Fig 4C-D), but that LRVs were observed even when using a *prfA** mutant strain. This strain carries a *prfA* allele encoding a PrfA variant with a G145S substitution that has been previously described to be constitutively active, and to lead to the strong overexpression of PrfA-dependent virulence genes, including that of *hlyA* (Ripio *et al*, 1997). Accordingly, the *in-vitro* haemolytic titre of the *prfA* strain we used was $10^5$-fold higher than that of the WT strain (Appendix Fig S2). Highly elevated levels of LLO

thus did not impede the ability of *Lm* to reside and multiply inside LRVs for several hours. This feature is contrasting with the properties of SLAPs previously described in phagocytes, which required moderate amounts of LLO secretion for their formation (Birmingham *et al*, 2008). Nevertheless, LLO hyperproduction facilitated bacterial escape from LRVs to a certain extent. Indeed, we observed in live-cell imaging (Fig 4C-D) that the very high levels of LLO secretion of the *prfA** strain hastened *Lm* escape from LRVs. In agreement with this result, the proportion of bacteria that replicated inside LRVs was lower when cells were infected with the *prf*A* strain than with the WT strain (Fig 4E).

Although the presence of LLO was not required for LRV formation and *Lm* escape, we observed that the *ΔhlyA Lm* strain was unable to proliferate inside LRVs (Fig 4C). Individual tracking of LRVs revealed that *Δhly*A bacteria barely grew when no LLO was secreted (Fig 4D). Similarly with SLAPs, LRVs thus required that bacteria secreted LLO to allow intravacuolar growth. The quantity of secreted LLO did not appear to affect bacterial growth, since the *prfA** strain replicated with a similar rate as the WT strain (Fig 4D). Consistently, the growth rate of LLO-FAST-secreting bacteria in LRVs was correlated with neither the average concentration (Appendix Fig S3C) nor the maximal level of LLO secretion (Appendix Fig S3D).

## Origin and properties of *Listeria* long residence vacuoles in epithelial cells

The LRVs in which *Lm* replicated (Fig 4) likely originated from internalisation vacuoles from which bacteria had failed to escape (Fig 3D). However, one cannot exclude that the vacuoles where *Lm* were found to replicate after 2 h p.i. might instead derive from secondary vacuoles produced by cell-to-cell spread, or by autophagy vacuoles where bacteria would have been entrapped after a first exposure to the cytoplasm. To assess if the LRVs where *Lm* proliferated were actually primary vacuoles, we monitored by confocal spinning disk fluorescence microscopy the intravacuolar stages of mCherry-expressing bacteria, in LoVo cells transfected by the YFP-CBD fusion protein reporter (Henry *et al*, 2006). This reporter has been previously described to specifically label the surface of bacteria that have once been exposed to the host cytoplasm, because the cell wall-binding domain (CBD) from the *Lm* phage endolysin Ply118 binds the cell wall of *Lm* with high affinity. Bacteria that replicated within LRVs remained unlabelled with YFP-CBD, until the vacuole ruptured and bacteria dispersed throughout the cytosol (Fig 5A, Movie EV6). This result rules out the possibility that bacteria underwent canonical autophagy or cell-to-cell spread after a first exposure to the host cell cytoplasm, and thereby confirms that LRVs where *Lm* replicates derive from internalisation vacuoles.

Because the replication compartments we observed were reminiscent of the SLAPs, we hypothesized that they could originate from a process analogous to LC3-accosiated phagocytosis (LAP), except it would occur in epithelial cells rather than in phagocytes. We thus endeavoured to better characterize this intravacuolar replication niche, and analyse whether it had typical features of endosomal, lysosomal and/or noncanonical autophagy-derived compartments. By immunofluorescence staining of LoVo cells infected with mCherry-expressing *Lm* for 3 hours, we observed that the vacuoles containing several bacteria were negative for the

early endosomal marker Rab5, while they were positive for the late endosomal marker Rab7, the lysosomal marker LAMP1, as well as LC3 (Fig 5B). These are typical markers of SLAPs, suggesting that, similar to what occurs in phagocytes, LC3 could be lipidated and the noncanonical autophagy machinery recruited to the entry vacuole in epithelial cells. In spite of the presence of the lysosomal marker LAMP1, the pH inside the LRVs remained neutral, as revealed by their absence of staining when using the acidophilic fluorescent probe LysoTracker Deep Red (Fig 5B). Altogether, we conclude that epithelial LRVs display molecular characteristics highly reminiscent of SLAPs, even though they allow a faster replication of *Lm*, and their maturation and rupture is less sensitive to the concentration of secreted LLO than the compartments observed in phagocytes.

# Discussion

Addressing the dynamics of secreted virulence factors at the (sub-)cellular scale constitutes one of the main challenges for real-time microscopy of infectious processes. Here, we brought evidence that FAST offered a versatile, convenient opportunity for tackling this challenge. We took advantage of it to measure the lifetime of *Lm* internalisation vacuoles, and to monitor the vacuolar localisation of the secreted *Lm* virulence factor LLO in live cells.

## Real-time imaging of LLO during infection

On fixed samples, addressing the localisation of LLO in infected cells has often constituted a hurdle, due to the poor quality of the labelling allowed by existing anti-LLO antibodies in immunofluorescence assays (e.g. Henry *et al*, 2006). LLO localisation at vacuole membranes, or more recently in bacterial-derived membrane vesicles, has been addressed by electron microscopy using immunogold labelling (Quinn *et al*, 1993; Coelho *et al*, 2018). However, the precise dynamics of infectious processes are not addressed with fixed-cell studies. In addition, the high special resolution gained by electron microscopy limits the overview of events at a cellular scale. As a complementary approach, LLO-eGFP fusions that were ectopically-expressed in host cells enabled live imaging studies, which yielded precious insight into the dynamics of LLO localisation at membranes and turnover (Chen *et al*, 2018). Nevertheless, such studies remained limited by expression from a transfected plasmid, which could not reproduce the concentrations, precise localisation and orientation of the insertion of LLO oligomers into vacuole membranes that are obtained with endogenous bacterial secretion. In addition, in non-infected cells, host cell signalling pathways and membrane dynamics do not undergo the same perturbations as in infected cells. Here, we report (*a*) that the FAST system can be used to tag LLO without loss of function, (*b*) that the LLO-FAST fusion can be expressed under its endogenous promoter and secreted by *Lm* in infected cells, (c) that the vacuoles it decorates can be imaged with accuracy, and (*d*) that some of these vacuoles unexpectedly last for several hours.

## LRVs, an alternative replication niche for *Listeria monocytogenes*

We observed that in LoVo epithelial cells, a consistent proportion of *Lm* failed to escape from the internalisation vacuole, but instead remained and replicated efficiently inside LRVs, which were positively labelled by LLO-FAST. The decoration of these compartments by LC3, Rab7 and LAMP1 as well as their neutral pH were reminiscent of the SLAPs previously described in phagocytes (Birmingham *et al*, 2008), and which derive from LAP (Mitchell *et al*, 2018). To our knowledge the LAP of *Lm* has not been previously reported to occur in epithelial cells, in contrast with *Sf* that can take advantage of a process similar to LAP (Schille *et al*, 2017). We thus propose a model for the formation of replicative LRVs in epithelial cells, analogous to the current model of SLAP formation (Fig 6). After its uptake by receptor-mediated endocytosis, the entrapment of *Lm* inside entry vacuoles could result in two distinct fates. (**A**) In the classically-described pathway, the coordinated actions of LLO and of the phospholipases PlcA and PlcB result in a rapid disruption of the vacuole and escape of bacteria into the cytoplasm, where they can start replicating and polymerising actin. (**B**) In the second scenario, a proportion of internalisation vacuoles would undergo LC3 lipidation in addition to their maturation attested by decoration with Rab7. The $LC3^+$, $Rab7^+$ endosomes would then fuse with lysosomes, as suggested by LAMP1 labelling. Membrane permeation by LLO might moderate the bactericidal properties of LRVs, and/or allow nutrient uptake through the permeated membrane, thereby promoting bacterial replication. After several hours of intravacuolar residence and growth, the membrane of LRVs eventually ruptured and the bacteria resumed the canonical cytosolic lifestyle.

Whereas the LRVs that we observed in LoVo cells displayed similarities with SLAPs, they were notably distinct from LisCVs, an intravacuolar persistence niche of *Lm* recently described in human hepatocytes and trophoblast cells (Kortebi *et al*, 2017). Indeed, contrary to LRVs and SLAPs, LisCVs did nor derive from primary vacuoles. Instead, they were described to form later during the intracellular cycle of *Lm*, by entrapment within vacuoles of bacteria having lost ActA-dependent motility. In line with this, bacteria found in LisCVs were labelled with YFP-CBD, while the bacteria we observed in LRVs were not. ActA function was indifferent to the formation of LRVs, since they were also observed when using a *prfA** strain, where *actA* is constitutively expressed (Reniere *et al*, 2015). Moreover, whereas LRVs were lipidated by LC3, LisCVs were LC3 negative. Last, the bacteria residing within LisCVs appeared to be in a viable, non-culturable state, while *Lm* replicated in LRVs. Altogether, though occurring in epithelial cells, the features we describe for LRVs are consistent with compartments similar to SLAPs, and distinct from LisCVs. However, the replication of *Lm* inside LRVs was significantly faster than the 8 hours of doubling time reported in SLAPs (Birmingham *et al*, 2008), perhaps due to a lower bactericidal capacity of the epithelial niche compared with phagocytes.

One question raised by the scenario depicted in Fig 6 resides in the mechanisms preserving the integrity of the primary vacuole over several hours, despite LLO secretion and the mechanical pressure exerted by growing bacteria. Similar observations using the *prfA** strain were even more surprising. Indeed, one would

anticipate that the excessive production of LLO by this strain would quickly destabilise vacuolar membranes (Ripio *et al*, 1997). In line with this view, in phagocytes *Lm* residence in SLAPs was favoured when using strains producing moderate amounts of LLO (Birmingham *et al*, 2008). One possible explanation for this difference would be if active repair mechanisms were at play in LoVo cells, bringing additional membrane components to the growing compartments. Whether the recruitment of lipidated LC3 and noncanonical autophagy is involved in this process might be a track for future investigations. As an alternative, rapid scavenging of LLO, made possible by its PEST sequence (Chen *et al*, 2018), could participate in maintaining a balance between vacuole permeation and rupture.

The relevance of LRVs in the context of infections remains to be explored. One possible aspect to be examined in future studies is to which extent this additional replicative niche contributes to the survival of *Lm* within epithelial cells and tissues, not only in LoVo epithelial cells but also in possible *in vivo* niches, and to the maintenance of an equilibrium between bacterial fitness, host responses and host-inflicted damage. Innate immune sensing of the pathogen would likely differ when *Lm* is thus entrapped, which could modulate the bacterial-host interplay. Vacuolar bacteria that cannot spread from cell to cell might also constitute chronic forms of infections by dampening immediate damage to the host. Together with LisCVs, with SLAPs, and with growth-restricting-processes associated with xenophagy (Mitchell *et al*, 2018), the LRVs we describe here in LoVo cells thus add-up to the notion that a variety of *Lm* intravacuolar forms may coexist in infected cells, each contributing to the complexity in sorting out possible outcomes of the infectious process.

## FAST, a versatile fluorescent reporter of bacterial secretion

Beyond the progress allowed for live detection of LLO and the description of this replicative compartment, the FAST reporter appears as a promising tool for live imaging studies of bacterial secretions adapted to a broad range of bacterial models and secretion systems. As a possible application, we have shown here that the simple accumulation of secreted FAST into *Lm* internalisation vacuoles allowed single particle tracking of these compartments, from the moment of their formation to the moment of their rupture, and thereby provided an accurate estimate of their lifetimes. Additionally, the fluorescent signal from secreted FAST inside the host cytoplasm could provide an estimation of infection heterogeneity among a cell population.

In recent years, several strategies have emerged for fluorescent labelling of Sec– or T3SS– dependent substrates (reviewed in O'Boyle *et al*, 2018). Tagging bacterial effectors with Split-GFP provides a possible solution that has been successfully applied for live detection of *Salmonella* T3SS-dependent effectors or *Listeria* Sec-dependent secreted substrates (Van Engelenburg & Palmer, 2010; Batan *et al*, 2018); however, the reconstitution process is slow compared with microbial growth, and requires the stable expression of GFP1-10 in recipient cells, which limits its application in most biological systems. Superfolder GFP (sfGFP) or its derivative rsFolder have been successfully used for labelling *E. coli* periplasmic proteins exported

through the Sec pathway (Dinh & Bernhardt, 2011; Peters *et al*, 2011; Dammeyer & Tinnefeld, 2012; Khatib *et al*, 2016), but to our knowledge has not been applied yet for other bacterial systems or in the context of host-pathogen interactions. Other fluorescent tags such as FlAsH and phiLOV were successfully used for monitoring the secretion of *Sf* T3SS-dependent effectors (Enninga *et al*, 2005; Gawthorne *et al*, 2016). Nevertheless, the toxicity in eukaryotic cells of the biarsenite dye used for FlAsH labelling and the rather modest brightness of phiLOV hamper their general use.

FAST compares with previously existing tools, while broadening the possible range of applications, due to (*a*) its ease of implementation (compared with Split-GFP); (*b*) its low toxicity (compared with FLASH); (*c*) its independence to oxygen (Monmeyran *et al*, 2018; Streett *et al*, 2019) as well as (*d*) its rapid and reversible folding dynamics allowing transport through the T3SS (compared with all GFP-derived probes); (*e*) its reasonable brightness and fast maturation time (compared with PhiLOV). In addition, FAST offers the opportunity to image secreted proteins at different wavelengths between 540 and 600 nm by selecting the appropriate fluorogen (Li *et al*, 2017), thereby providing users with flexibility in the choice of other fluorescent reporters in co-localisation studies. Red-shifted fluorogens also limit the toxicity of certain wavelength for bacteria when performing long-term imaging. Membrane-impermeant fluorogens potentially also grant the possibility to discriminate between intracellular and extracellular proteins (Li *et al*, 2018), for instance when addressing the localisation of bacterial effectors that anchor to the bacterial cell wall or to membranes.

In conclusion, FAST expands the panel of fluorescent reporters adapted for tracking secreted virulence factors, with promises of novel application perspectives in a variety of biological contexts. Indeed, with only minor changes in the setup, FAST could be adapted to the live imaging of a vast array of surface proteins and diffusible factors secreted by various microorganisms, including anaerobes. Beyond the infection of cultured cells, deeper microscopy on infected organ explants can be foreseen. This would generate a wealth of opportunities to accurately depict the spatiotemporal aspects of infection mechanisms.

# Material and methods

## Bacterial strains, plasmids and culture conditions

The bacterial source strains used in this work were *Escherichia coli* NEB5α (New England Biolabs) for plasmid constructions, Rosetta(DE3)pLysS (Novagen) for recombinant protein production, the clinical isolate of *Listeria monocytogenes* LL195 (lineage I, ST1) (Weinmaier *et al*, 2013) for most of the experiments involving *Lm*, and *Shigella flexneri* M90T (Sansonetti *et al*, 1982) for experiments on *Sf* T3SS-dependent secretion. *Lm* reference strain EGD-e (lineage 2, ST9) (Glaser *et al*, 2001) (lineage II, ST9) was also used as a control that the observed vacuolar phenotype was not specific to LL195. All strains were grown at 37°C under shaking at 190 rpm in Luria Bertani (LB) medium for *E. coli*, in LB or tryptic soy broth (TSB) for *Sf*, in brain hear infusion (BHI) or incomplete *Listeria* synthetic medium (Whiteley *et al*, 2017) for

*Lm*. Whenever required, media were supplemented with antibiotics for plasmid selection (chloramphenicol, 35 µg/ml for *E. coli*; 20 µg/ml for *Sf*; 7 µg/ml for *Lm* or Ampicillin, 100 µg/ml), or Congo red (1 mg/ml) for activation of the *Sf* T3SS.

In order to favour the expression of transgenes, the DNA coding sequence for FAST, fused with a Myc-tag, was codon-optimized for *Lm* (gfAL001, Appendix Fig S1A) or *Sf* (gfAL002, Appendix Fig S1B) using the online Optimizer application (http://genomes.urv.es/OPTIMIZER/) in guided random mode. The optimized sequences were obtained as synthetic Gene Fragments (Eurofins genomics). gfAL001 additionally contained the 5'-untranslated (5'-UTR) of the *hlyA* gene, and the sequence encoding the signal peptide (SP) of LLO in its N-terminal part.

For plasmid constructions in the pPL2 backbone (Fig EV1), gfAL001 was amplified with primers oAL543-4, the sequence of the *Lm hlyA* gene encoding LLO was amplified from the EGD-e genomic DNA with primers oAL549-50b, and the coding sequence for eGFP was amplified from pAD-cGFP (BUG2479) (Balestrino *et al*, 2010) with primers oAL543-7. The $UTR_{hlyA}$-SP-FAST-Myc amplicon was inserted instead of $UTR_{hlyA}$-eGFP into the *Eag*I-*Sal*I restriction sites of pAD-cGFP, thus generating pAD-SP-FAST, where FAST is under control of the $P_{HYPER}$ constitutive promoter (Fig EV1A). pAD-FAST, pAD-eGFP, pAD-SP-eGFP, pAD-LLO, pAD-LLO-FAST and pAD-LLO-eGFP, all containing the 5'-UTR of *hlyA* and a Myc tag, were likewise generated by inserting the cognate DNA amplicons into the same restriction sites (Fig EV1A). After cloning in *E. coli* NEB5α, these plasmids were integrated in the genome of *L. monocytogenes* strains LL195 at the $tRNA^{Arg}$ locus as previously described (Lauer *et al*, 2002).

For allelic replacement at the *hlyA* locus (Fig EV1C), pMAD-Δ*hlyA*::FAST was created by amplifying three partially overlapping fragments by PCR: One thousand base pairs (bp) upstream (*plcA* gene) and downstream (*mpl* gene) of the *hlyA* open reading frame in the EGD-e genome were amplified, respectively, with oAL981-2 and oAL976-7, while the FAST-Myc open reading frame was amplified from pAD-FAST with oAL983-75. These fragments were inserted into the pMAD vector between the *Sal*I and *Bgl*II restriction sites by Gibson Assembly, using the NEBuilder HiFi DNA Assembly Cloning Kit (New England BioLabs). pMAD-*hly*A-FAST containing the last 1000 bp of *hlyA* fused with the FAST sequence, a Myc tag and one thousand bp downsteream of *hlyA* was likewise generated by inserting the cognate DNA amplicons into the same restriction sites in pMAD. Allelic replacements of the *hlyA* open reading frame by these constructs in the genomes of *L. monocytogenes* strains LL195 and EGD-e were obtained as previously described (Trieu-Cuot *et al*, 1991). For complementation purposes in haemolysis assays, a simple in-frame deletion mutant of the *hlyA* gene was also created using the pMAD backbone.

For *Sf* constructs, *ipaB* and *ospF* were amplified from M90T genomic DNA with primers oAL703-4 and 707-8 respectively, and gfAL002 was amplified with primers oAL705-6. pSU2.1-OspF-FAST (Fig EV1B) was obtained by inserting an oAL707-6 amplicon overlapping *ospF* and FAST-Myc, with a *Bam*HI restriction linker, in place of mCherry into the *Kpn*I-*Xba*I restriction sites of pSU2.1rp-mCherry (Campbell-

Valois *et al*, 2015). pSU2.1-IpaB-FAST was generated by replacing *ospF* with *ipaB* (oAL703-4) at the *Kpn*I-*Bam*HI sites (Fig EV1B). After cloning in *E. coli* NEB5α, these plasmids were introduced in *Sf* M90T by electroporation.

The complete lists of bacterial strains and oligonucleotides used in this work are supplied as Appendix Tables S1 and S2, respectively.

## Bacterial total extracts or secreted protein analysis

Bacterial total extracts or culture supernatants were recovered from 1 ml of *Lm* strains grown to a $OD_{600nm}$ of 2.0 in BHI medium at 37°C as previously described (Lebreton *et al*, 2011).

Total bacterial extracts of *Sf* were prepared by boiling for 2 × 10 min at 95°C in 100 µl of Laemmli sample buffer (SB 1X) the bacterial pellets obtained by centrifugation of 1 ml of each strain grown to a $OD_{600nm}$ of 2.0 in TCS medium at 37°C. For assessment of secretion leakage prior to T3SS induction, 2 ml of *Sf* culture supernatants were collected, precipitated with 16% trichloroacetic acid (TCA), and centrifuged for 30 min at 16,000 × *g* at 4°C. Protein pellets were washed twice in acetone before resuspension in 50 µl of SB 1X. For induction of secretion, *Sf* were resuspended in 0.6 ml phosphate buffered saline (PBS) containing 1 mg/ml of Congo red at a final $OD_{600nm}$ of 40, and incubated at 37°C for 45 min. Bacteria were eliminated by centrifugation; 100 µl of supernatant were collected and mixed with 33 µl of SB 4X for SDS-PAGE separation. The remainder supernatant was TCA-precipitated and resuspended in 50 µl SB 1X as above.

10 µl of each sample were separated on 4-15% Mini-Protean TGX gels (Bio-Rad) by sodium dodecyl sulfate-polyacrylamide gel electrophoresis (SDS-PAGE). For immunoblots, after transfer on nitrocellulose membrane (Amersham) using PierceG2 Fast Blotter, proteins were probed with anti-Myc mouse monoclonal antibody #9E10 (sc-40, Santa Cruz Biotechnology) at a 1:400 dilution in PBS supplemented with 0.05% tween-20 and 5% skimmed milk powder, followed by secondary hybridization with anti-Mouse IgG-heavy and light chain Antibody (Bethyl) at a 1:50 000 dilution in the same buffer. Signals were detected using Pierce ECL Plus Western Blotting Substrate and a Las4000 imager (GE Healthcare). Staining with colloidal Coomassie Brillant blue G-250 was performed as previously described (Neuhoff *et al*, 1988).

## Haemolysis assay

The supernatants of overnight-grown cultures of *Lm* in BHI medium were recovered by centrifugation for 1 min at 6,000 × *g* followed by filtration through 0.2-µm pore filters, in order to eliminate bacteria. Serial two-fold dilutions of these supernatants were performed in round-bottom, clear, 96-well plates (100 µl final volume per well) using as a diluent PBS, the pH of which was adjusted to 5.6, and supplemented with 0.1% bovine serum albumin (BSA). Erythrocytes from defibrinated mice blood were washed twice in PBS pH 6.4 and diluted $1/10^{th}$ in PBS pH 5.6. 50 µl of this suspension was added to each one of the wells containing diluted culture supernatants. After 30 min of incubation at 37°C, the plates were centrifuged for 10 min at

430 × *g* and haemolytic titres were calculated as the reciprocal of the dilution for which 50% of haemolysis was observed (Roche *et al*, 2001).

## Fluorescence measurement on culture supernatants

*Lm* were grown overnight in BHI, washed and diluted to 1:10$^{th}$ in iLSM, and then grown for 6 h at 37°C, 180 rpm. Likewise for secretion by *Sf*, a culture in TSB was diluted to 1:10$^{th}$ in M9 medium supplemented with 0.2% glucose and 10 µg/ml nicotic acid. From 1 ml of culture, bacterial pellets were collected by centrifugation of the cultures at 6,000 × *g*, then washed in PBS and resuspended in 1 ml of PBS. The culture supernatants were filtered (0.2 µm pores). For fluorescence measurements of FAST-tagged fusions, 180 µl of each sample was mixed with 20 µl of 50 µM HBR-3,5-DM ((*Z*)-5-(4-Hydroxy-3,5-dimethylbenzylidene)-2-thioxothiazolidin-4-one) to obtain a final concentration of 5 µM of fluorogen. 20 µl of PBS were used for negative controls, where no fluorescence was detected above that of the control medium (iLSM where *Lm* producing the non-fluorescent fusion LLO-Myc were grown, or supplemented M9 medium of a culture of *Sf* M90T Δ*ipaD*). Fluorescence intensity of technical triplicates was measured on a Spark 10M multimode microplate reader (Tecan), with excitation/emission wavelength set to 499/562 nm for FAST:HBR-3,5-DM; 488/507nm for eGFP. After subtraction of background fluorescence corresponding to the negative control strains, fluorescence values in culture media were expressed as a percentage of the fluorescence measured for the suspension of bacteria expressing either non-secreted FAST, or eGFP (for *Lm*), or of M90T WT expressing OspF-FAST or IpaB-FAST (for *Sf*).

The standard curve for FAST fluorescence quantification was performed by diluting, in control medium, known amounts of recombinant FAST produced in *E. coli* Rosetta(DE3)pLysS as previously described (Plamont *et al*, 2016).

Each experiment was reproduced three times independently.

## Infection and transfection of epithelial cells

Infections of intestinal epithelial cells were performed in the LoVo cell line originating from colon adenocarcinoma (ATCC CCL-229), grown in Ham's F-12K medium supplemented with 10% FBS, following ATCC recommendations. The Caco-2 epithelial cell line (ATCC HTB-37), also from colon adenocarcinoma, was used as a control that LRVs were not a specificity of LoVo cells. All cells were cultured at 37°C in a humidified atmosphere containing 5% $CO_2$. For live microscopy, cells were seeded on Ibidi µslides 72 h prior to infection at a density of $10^5$ cells/ml, in 300 µg/ml of culture medium. When needed, cells were transfected 24 h before infection with pEYFP-C1-CBD expressing YFP-CBD (Henry *et al*, 2006), using Lipofectamine LTX (Invitrogen) and 1 µg/ml of plasmid, according to the manufacturer's specifications.

*Lm* strains were grown in BHI medium until they reached early stationary phase ($OD_{600}$ of 2 to 3), washed

in pre-warmed D-MEM, and then diluted in culture medium without serum to achieve a multiplicity of infection (MOI) of 5 (for long-term infections) to 30 (for short-term infections). Except for short-term imaging when bacterial entry was monitored under the microscope, after 30 min of bacteria-cell contact the inoculum was washed away by washing cells twice with serum-free medium containing 40 µg/ml of gentamicin, then the medium was replaced by complete culture medium without phenol red containing 25 µg/ml in order to kill extracellular bacteria.

## Live fluorescence microscopy of infected cells

Cells infected as described above were observed in D-MEM without phenol red supplemented with 10% of FBS, 5 µM of HBR-3,5-DM for fluorescence detection, 250 nM of the fluorogenic probe SiR-actin for actin detection, and 25 µg/ml of gentamicin for long-term infections. For experiments where early events were monitored, the labelling of actin by SiR-actin was initiated 2 h prior to infection by adding 250 nM of SiR-actin to the medium.

For live cell imaging, preparations were observed with a Nikon Ti PFS microscope coupled to a spinning disk confocal device (CSU-XI-A1, Yokogawa), connected to a cooled EM-CCD camera (Evolve, Photometrics), and equipped with a Cube for temperature control and a Brick gas mixed for a $CO_2$ and humidity control (Life Imaging Services). Image acquisition and microscope control were actuated with the MetaMorph software (Molecular Devices). Fluorescent illumination was driven by three lasers, of wavelength 491 nm for eGFP, YFP of FAST, 561 nm for mCherry, and 635 nm for SiR-actin. Images were acquired with apochromat 63x objective lenses (NA 1.4) in 1 µm step-Z-stacks. Acquisition parameters were similar for all samples of an experiment. For snapshot display, maximum intensity signals from 16 successive stacks (i.e. 16 µm slices) were integrated with Fiji. Each picture or video is representative of the population observed in three independent experiments.

For measurement of FAST accumulation in cells, images were first z-projected by maximum intensity, then fluorescence intensities were quantified on regions of fixed areas using Fiji. Vacuole tracking and bacterial growth rate calculations were performed using Matlab scripts tailored to each purpose as detailed below.

## Tracking of primary vacuoles in short term infection assays

The slices of the z-stack obtained from spinning confocal imaging were projected onto a single plane (maximal projection). Fluorescent vacuoles were tracked using the plugin TrackMate in Fiji. The time at which tracks began during the infection was used to compute the time of *Lm* entry into LoVo cells. We then reconstructed the cumulative distribution of entries as a function of time and the entry rate was obtained by fitting the slope of the linear cumulative distribution of entries with time. Finally, the distribution of residence times in primary vacuoles was computed from the statistics of track length.

## Tracking of LRVs in long-term infection assays

At 2 h p.i., Ibidi µslides were mounted on a confocal spinning disc microscope for observations. The mCherry signal labelling the bacterial cytoplasm was used to segment the volume of bacteria. Given the good signal-to-noise ratio of mCherry images, we performed a direct Otsu-thresholding algorithm on the mCherry stacks to obtain the 3D segmentation of bacteria. We then used MatLab routines to track objects based on their size and their location. To measure LLO-FAST signals in primary vacuoles, we applied on the FAST images the binary masks retrieved from mCherry segmentation and computed the average FAST signal in each mask. The fraction of the primary vacuoles into which *Lm* replicated was computed as the ratio of the number of tracked vacuoles that at least doubled their size during the course of the movie (12 h) to the initial number of bacteria. The growth rates of bacteria inside LRVs were computed by fitting the dynamics of segmented mCherry volumes to an exponential function.

## Immunofluorescence or LysoTracker staining of infected cells

LoVo cells were seeded 48 h before infection in 24-well plates containing 12 mm diameter coverslips pre-coated with poly-L-lysine. Infection with bacteria expressing mCherry (for immunofluorescence experiments) or eGFP (for LysoTracker staining) was performed as described above, using a MOI of 30, except that plates were centrifuged for 1 min at 200 × *g* after addition of the inoculum in order to synchronise bacteria-cell contacts. 3 h p.i., cells were washed in pre-warmed PBS, fixed 20 min with 4% paraformaldehyde in PBS, then permeabilized for 5 min at room temperature with 0.5% Triton X-100 in PBS, and blocked for 5 min in PBS buffer containing 2 % bovine serum albumin (BSA, Sigma). Incubation with primary antibodies in PBS buffer, 1 % BSA was performed for 1 h, followed by three PBS washes, and incubation with the Alexa Fluor 647-conjugated secondary anti-rabbit antibody (Molecular probes #A21245, 2 µg/µl), Acti-stain 488 fluorescent phalloidin (Cytoskeleton #PHDG1, 70 nM) and DAPI (0.1 µg/µl) for 30 min. After three additional washes, cover glasses were finally mounted on microscope slides with Fluoromount mounting medium (Interchim). Rabbit monoclonal primary antibodies from Cell Signalling Technologies against Rab5 (#3547) and LAMP1 were used at a 1:200 dilution (#9367); rabbit polyclonal antibodies against LC3 (MBL International #PM036) were used at a 1:500 dilution.

Staining of acidic compartments was obtained by adding 50 nM of LysoTracker Deed Red (Molecular Probes #L12492) to the cell culture medium 1 h prior to observation. Infected cells were then observed in DMEM without phenol red, supplemented with 500 ng/ml Hoechst 33342 and 25 µg/ml gentamicin.

Preparations were observed with a Nikon Ti epifluorescence microscope (Nikon), connected to a digital CMOS camera (Orca Flash 4.0, Hamamatsu). Illumination was achieved using a SOLA-SE 365 source (Lumencor) and the following excitation/emission/dichroic filter sets (Semrock): DAPI or Hoechst, 377(50)/447(60)/FF409-Di03 ; Acti-Stain 488 or eGFP, 472(30)/520(35)/FF495-Di03 ; mCherry, 562(40)/632(22)/dic FF562-Di03; Alexa 647 or LysoTracker, 630(30)/684(24)/dic FF655-Di01. Images

were acquired with Nikon apochromat 60x objective lenses (NA 1.4). Image acquisition and microscope control were actuated with the μManager software, and processed with Fiji. Each picture is representative of the infected cell population.

## Acknowledgements

We are grateful to Marie-Aude Plamont, Vinko Besic, Sebastian Rupp and Alison Tebo for their precious experimental assistance and eagerness to help solve technical issues. We thank Lionel Schiavolin and Didier Filopon for providing source strains and practical advice regarding *Sf* experiments. We thank the IBENS imaging facility for maintaining access to microscopy equipment that was instrumental to this work, and providing expert support whenever needed. We are indebted to the IBENS animal facility for kindly supplying the mice blood used in haemolysis assays. We thank Jost Enninga for renewed proofs of enthusiasm and insightful discussion.

## Author contributions

AL, ND, AG designed the project. CPC, AL, ND, AG designed experiments and interpreted results. CPC, AL, ND, JL, LW, JCF performed experiments. CPC, ND analysed data. AL and ND wrote the manuscript with input from CPC and AG.

## Funding

Work in the group of AL has received support under the program "Investissements d'Avenir" implemented by ANR (ANR-10-LABX-54 MemoLife and ANR-10-IDEX-0001-02 PSL University), Fondation pour la Recherche Médicale (FRM-AJE20131128944), Inserm ATIP-Avenir and Mairie de Paris (programme Émergences – Recherche médicale). CPC received a doctoral fellowship from programme Interface pour le Vivant from Sorbonne University.

## Declaration of interests

The authors declare the following competing financial interest: AG is co-founder and holds equity in Twinkle Bioscience/The Twinkle Factory, a company commercializing the FAST technology.

## References

Balestrino D, Hamon MA, Dortet L, Nahori M-A, Pizarro-Cerda J, Alignani D, Dussurget O, Cossart P & Toledo-Arana A (2010) Single-cell techniques using chromosomally tagged fluorescent bacteria to study *Listeria monocytogenes* infection processes. *Appl Environ Microbiol* **76:** 3625–3636

Batan D, Braselmann E, Minson M, Nguyen DMT, Cossart P & Palmer AE (2018) A multicolor split-fluorescent protein approach to visualize *Listeria* protein secretion in infection. *Biophys. J.*

Beauregard KE, Lee KD, Collier RJ & Swanson JA (1997) pH-dependent perforation of macrophage phagosomes by listeriolysin O from *Listeria monocytogenes*. *J Exp Med* **186:** 1159–1163

Birmingham CL, Canadien V, Kaniuk NA, Steinberg BE, Higgins DE & Brumell JH (2008) Listeriolysin O allows *Listeria monocytogenes* replication in macrophage vacuoles. *Nature* **451:** 350–354

Burrack LS, Harper JW & Higgins DE (2009) Perturbation of vacuolar maturation promotes listeriolysin O-independent vacuolar escape during *Listeria monocytogenes* infection of human cells. *Cell Microbiol* **11:** 1382–1398

Campbell-Valois F-X, Sachse M, Sansonetti PJ & Parsot C (2015) Escape of Actively Secreting *Shigella flexneri* from ATG8/LC3-Positive Vacuoles Formed during Cell-To-Cell Spread Is Facilitated by IcsB and VirA. *MBio* **6:** e02567–14–14

Chen C, Nguyen BN, Mitchell G, Margolis SR, Ma D & Portnoy DA (2018) The Listeriolysin O PEST-like Sequence Co-opts AP-2-Mediated Endocytosis to Prevent Plasma Membrane Damage during *Listeria Infection*. *Cell Host Microbe* **23:** 786–795.e5

Coelho C, Brown LC, Maryam M, Vij R, Smith DF, Burnet MC, Kyle JE, Heyman HM, Ramirez J, Prados-Rosales R, Lauvau G, Nakayasu ES, Brady NR, Hamacher-Brady A, Coppens I & Casadevall A (2018) *Listeria monocytogenes* virulence factors, including Listeriolysin O, are secreted in biologically active extracellular vesicles. *J Biol Chem***:** jbc.RA118.006472

Cossart P & Lebreton A (2014) A trip in the 'New Microbiology' with the bacterial pathogen *Listeria monocytogenes*. *FEBS Lett* **588:** 2437–2445

Dammeyer T & Tinnefeld P (2012) Engineered fluorescent proteins illuminate the bacterial periplasm. *Computational and Structural Biotechnology Journal* **3:** e201210013

Di Russo Case E & Samuel JE (2016) Contrasting Lifestyles Within the Host Cell. *Microbiology Spectrum* **4:** 667–692

Dinh T & Bernhardt TG (2011) Using superfolder green fluorescent protein for periplasmic protein localization studies. *J Bacteriol* **193:** 4984–4987

Enninga J, Mounier J, Sansonetti PJ & Tran Van Nhieu G (2005) Secretion of type III effectors into host cells in real time. *Nat Methods* **2:** 959–965

Gawthorne JA, Audry L, McQuitty C, Dean P, Christie JM, Enninga J & Roe AJ (2016) Visualizing the translocation and localization of bacterial type III effector proteins by using a genetically encoded reporter system. *Appl Environ Microbiol* **82:** 2700–2708

Glaser P, Frangeul L, Buchrieser C, Rusniok C, Amend A, Baquero F, Berche P, Bloecker H, Brandt P, Chakraborty T, Charbit A, Chetouani F, Couvé E, de Daruvar A, Dehoux P, Domann E, Domínguez-Bernal G, Duchaud E, Durant L, Dussurget O, et al (2001) Comparative genomics of *Listeria* species.

*Science* **294:** 849–852

Gouin E, Welch MD & Cossart P (2005) Actin-based motility of intracellular pathogens. *Curr. Opin. Microbiol.* **8:** 35–45

Henry R, Shaughnessy L, Loessner MJ, Alberti-Segui C, Higgins DE & Swanson JA (2006) Cytolysin-dependent delay of vacuole maturation in macrophages infected with *Listeria monocytogenes*. *Cell Microbiol* **8:** 107–119

Khatib El M, Martins A, Bourgeois D, Colletier J-P & Adam V (2016) Rational design of ultrastable and reversibly photoswitchable fluorescent proteins for super-resolution imaging of the bacterial periplasm. *Sci Rep* **6:** 92

Kortebi M, Milohanic E, Mitchell G, Péchoux C, Prevost M-C, Cossart P & Bierne H (2017) *Listeria monocytogenes* switches from dissemination to persistence by adopting a vacuolar lifestyle in epithelial cells. *PLoS Pathog* **13:** e1006734

Köster S, van Pee K, Hudel M, Leustik M, Rhinow D, Kühlbrandt W, Chakraborty T & Yildiz Ö (2014) Crystal structure of listeriolysin O reveals molecular details of oligomerization and pore formation. *Nat Commun* **5:** 3690

las Heras de A, Cain RJ, Bielecka MK & Vázquez-Boland JA (2011) Regulation of *Listeria* virulence: PrfA master and commander. *Curr. Opin. Microbiol.* **14:** 118–127

Lauer P, Chow MYN, Loessner MJ, Portnoy DA & Calendar R (2002) Construction, characterization, and use of two *Listeria monocytogenes* site-specific phage integration vectors. *J Bacteriol* **184:** 4177–4186

Lebreton A & Cossart P (2017) RNA- and protein-mediated control of *Listeria monocytogenes* virulence gene expression. *RNA biology* **14:** 460–470

Lebreton A, Lakisic G, Job V, Fritsch L, Tham TN, Camejo A, Matteï P-J, Regnault B, Nahori M-A, Cabanes D, Gautreau A, Ait-Si-Ali S, Dessen A, Cossart P & Bierne H (2011) A bacterial protein targets the BAHD1 chromatin complex to stimulate type III interferon response. *Science* **331:** 1319–1321

Li C, Mourton A, Plamont M-A, Rodrigues V, Aujard I, Volovitch M, Le Saux T, Perez F, Vriz S, Jullien L, Joliot A & Gautier A (2018) Fluorogenic Probing of Membrane Protein Trafficking. *Bioconjug. Chem.* **29:** 1823–1828

Li C, Plamont M-A, Sladitschek HL, Rodrigues V, Aujard I, Neveu P, Le Saux T, Jullien L & Gautier A (2017) Dynamic multicolor protein labeling in living cells. *Chem Sci* **8:** 5598–5605

Marquis H, Doshi V & Portnoy DA (1995) The broad-range phospholipase C and a metalloprotease mediate listeriolysin O-independent escape of *Listeria monocytogenes* from a primary vacuole in human epithelial cells. *Infect Immun* **63:** 4531–4534

Ménard R, Sansonetti PJ & Parsot C (1993) Nonpolar mutagenesis of the ipa genes defines IpaB, IpaC, and IpaD as effectors of *Shigella flexneri* entry into epithelial cells. *J Bacteriol* **175:** 5899–5906

Ménard R, Sansonetti PJ & Parsot C (1994) The secretion of the *Shigella flexneri* Ipa invasins is activated by epithelial cells and controlled by IpaB and IpaD. *EMBO J* **13:** 5293–5302

Mitchell G, Cheng MI, Chen C, Nguyen BN, Whiteley AT, Kianian S, Cox JS, Green DR, McDonald KL & Portnoy DA (2018) *Listeria monocytogenes* triggers noncanonical autophagy upon phagocytosis, but avoids subsequent growth-restricting xenophagy. *Proc Natl Acad Sci USA* **115:** E210–E217

Monmeyran A, Thomen P, Jonquière H, Sureau F, Li C, Plamont M-A, Douarche C, Casella J-F, Gautier A & Henry N (2018) The inducible chemical-genetic fluorescent marker FAST outperforms classical fluorescent proteins in the quantitative reporting of bacterial biofilm dynamics. *Sci Rep* **8:** 10336

Myers JT, Tsang AW & Swanson JA (2003) Localized reactive oxygen and nitrogen intermediates inhibit escape of *Listeria monocytogenes* from vacuoles in activated macrophages. *The Journal of Immunology* **171:** 5447–5453

Neuhoff V, Arold N, Taube D & Ehrhardt W (1988) Improved staining of proteins in polyacrylamide gels including isoelectric focusing gels with clear background at nanogram sensitivity using Coomassie Brilliant Blue G-250 and R-250. *Electrophoresis* **9:** 255–262

Nguyen BN, Peterson BN & Portnoy DA (2018) Listeriolysin O: a phagosome-specific cytolysin revisited. *Cell Microbiol***:** e12988

O'Boyle N, Connolly JPR & Roe AJ (2018) Tracking elusive cargo: Illuminating spatio-temporal Type 3 effector protein dynamics using reporters. *Cell Microbiol* **20:** e12797

Paz I, Sachse M, Dupont N, Mounier J, Cederfur C, Enninga J, Leffler H, Poirier F, Prevost M-C, Lafont F & Sansonetti PJ (2010) Galectin-3, a marker for vacuole lysis by invasive pathogens. *Cell Microbiol* **12:** 530–544

Peters NT, Dinh T & Bernhardt TG (2011) A fail-safe mechanism in the septal ring assembly pathway generated by the sequential recruitment of cell separation amidases and their activators. *J Bacteriol* **193:** 4973–4983

Pinaud L, Sansonetti PJ & Phalipon A (2018) Host Cell Targeting by Enteropathogenic Bacteria T3SS Effectors. *Trends Microbiol* **26:** 266–283

Pizarro-Cerda J & Cossart P (2018) *Listeria monocytogenes*: cell biology of invasion and intracellular growth. *Microbiology Spectrum* **6:**

Plamont M-A, Billon-Denis E, Maurin S, Gauron C, Pimenta FM, Specht CG, Shi J, Quérard J, Pan B, Rossignol J, Morellet N, Volovitch M, Lescop E, Chen Y, Triller A, Vriz S, Le Saux T, Jullien L & Gautier A (2016) Small fluorescence-activating and absorption-shifting tag for tunable protein imaging in vivo. *Proc Natl Acad Sci USA* **113:** 497–502

Quereda JJ, Pizarro-Cerda J, Balestrino D, Bobard A, Danckaert A, Aulner N, Shorte S, Enninga J & Cossart P (2015) A dual microscopy-based assay to assess *Listeria monocytogenes* cellular entry and vacuolar escape. *Appl Environ Microbiol* **82:** 211–217

Quinn F, Pine L, White E, George V, Gutekunst K & Swaminathan B (1993) Immunogold labelling of *Listeria monocytogenes* virulence-related factors within Caco-2 cells. *Res. Microbiol.* **144:** 597–608

Radoshevich L, Impens F, Ribet D, Quereda JJ, Nam Tham T, Nahori M-A, Bierne H, Dussurget O, Pizarro-Cerda J, Knobeloch K-P & Cossart P (2015) ISG15 counteracts *Listeria monocytogenes* infection. *Elife* **4:** 4153

Ray K, Bobard A, Danckaert A, Paz-Haftel I, Clair C, Ehsani S, Tang C, Sansonetti PJ, Van Nhieu GT & Enninga J (2010) Tracking the dynamic interplay between bacterial and host factors during pathogen-induced vacuole rupture in real time. *Cell Microbiol* **12:** 545–556

Reniere ML, Whiteley AT, Hamilton KL, John SM, Lauer P, Brennan RG & Portnoy DA (2015) Glutathione activates virulence gene expression of an intracellular pathogen. *Nature* **517:** 170–173

Ripio MT, Domínguez-Bernal G, Lara M, Suárez M & Vázquez-Boland JA (1997) A Gly145Ser substitution in the transcriptional activator PrfA causes constitutive overexpression of virulence factors in *Listeria monocytogenes*. *J Bacteriol* **179:** 1533–1540

Roche SM, Velge P, Bottreau E, Durier C, Marquet-van der Mee N & Pardon P (2001) Assessment of the virulence of *Listeria monocytogenes:* agreement between a plaque-forming assay with HT-29 cells and infection of immunocompetent mice. *Int. J. Food Microbiol.* **68:** 33–44

Ruan Y, Rezelj S, Bedina Zavec A, Anderluh G & Scheuring S (2016) Listeriolysin O Membrane Damaging Activity Involves Arc Formation and Lineaction — Implication for *Listeria monocytogenes* Escape from Phagocytic Vacuole. *PLoS Pathog* **12:** e1005597

Salcedo SP & Holden DW (2005) Bacterial interactions with the eukaryotic secretory pathway. *Curr. Opin. Microbiol.* **8:** 92–98

Sansonetti PJ, Kopecko DJ & Formal SB (1982) Involvement of a plasmid in the invasive ability of *Shigella flexneri*. *Infect Immun* **35:** 852–860

Schille S, Crauwels P, Bohn R, Bagola K, Walther P & van Zandbergen G (2017) LC3-associated phagocytosis in microbial pathogenesis. *Int J Med Microbiol* **308:** 228–236

Schuerch DW, Wilson-Kubalek EM & Tweten RK (2005) Molecular basis of listeriolysin O pH dependence. *Proc Natl Acad Sci USA* **102:** 12537–12542

Shen A & Higgins DE (2005) The 5' untranslated region-mediated enhancement of intracellular listeriolysin O production is required for *Listeria monocytogenes* pathogenicity. *Mol Microbiol* **57:** 1460–1473

Streett HE, Kalis KM & Papoutsakis ET (2019) A Strongly Fluorescing Anaerobic Reporter and Protein-Tagging System for Clostridium Organisms Based on the Fluorescence-Activating and Absorption-Shifting Tag Protein (FAST). *Appl Environ Microbiol* **85:** 714

Trieu-Cuot P, Carlier C, Poyart-Salmeron C & Courvalin P (1991) Shuttle vectors containing a multiple cloning site and a lacZα gene for conjugal transfer of DNA from *Escherichia coli* to Gram-positive bacteria. *Gene* **102:** 99–104

van der Ploeg R, Monteferrante CG, Piersma S, Barnett JP, Kouwen TRHM, Robinson C & van Dijl JM (2012) High-salinity growth conditions promote Tat-independent secretion of Tat substrates in *Bacillus subtilis*. *Appl Environ Microbiol* **78:** 7733–7744

Van Engelenburg SB & Palmer AE (2010) Imaging type-III secretion reveals dynamics and spatial segregation of *Salmonella* effectors. *Nat Methods* **7:** 325–330

Vincent WJB, Freisinger CM, Lam P-Y, Huttenlocher A & Sauer J-D (2016) Macrophages mediate flagellin induced inflammasome activation and host defense in zebrafish. *Cell Microbiol* **18:** 591–604

Weinmaier T, Riesing M, Rattei T, Bille J, Arguedas-Villa C, Stephan R & Tasara T (2013) Complete genome sequence of *Listeria monocytogenes* LL195, a serotype 4b strain from the 1983-1987 listeriosis epidemic in Switzerland. *Genome Announc* **1:** e00152–12–e00152–12

Whiteley AT, Garelis NE, Peterson BN, Choi PH, Tong L, Woodward JJ & Portnoy DA (2017) c-di-AMP modulates *Listeria monocytogenes* central metabolism to regulate growth, antibiotic resistance and osmoregulation. *Mol Microbiol* **104:** 212–233

# Figures

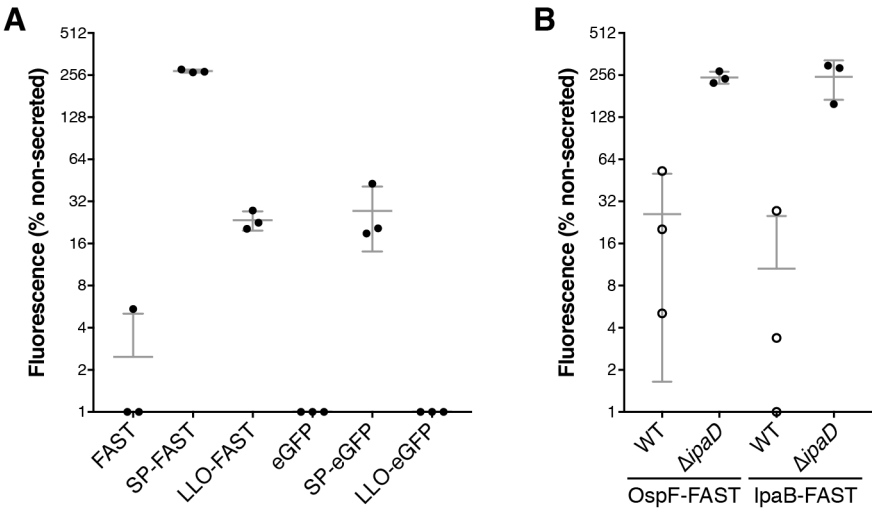


**Figure 1. FAST-tagged proteins retain fluorescent properties after secretion into bacterial culture media.**

Fluorescent signals generated by proteins secreted by *Lm* in iLSM (**A**) or by *Sf* in M9 medium (**B**) were measured in presence of 5 µM HBR-3,5-DM. Intensities were expressed as a percentage of the fluorescence measured in a corresponding suspension of *Lm* producing non-secreted FAST or eGFP (**A**), or of WT *Sf* producing OspF-FAST or IpaB-FAST, taken as a reference. All values below 1% of the reference were considered below the detection limit for this experiment, and represented as 1%. Normalized values, mean and standard deviations from three independent experiments were plotted.

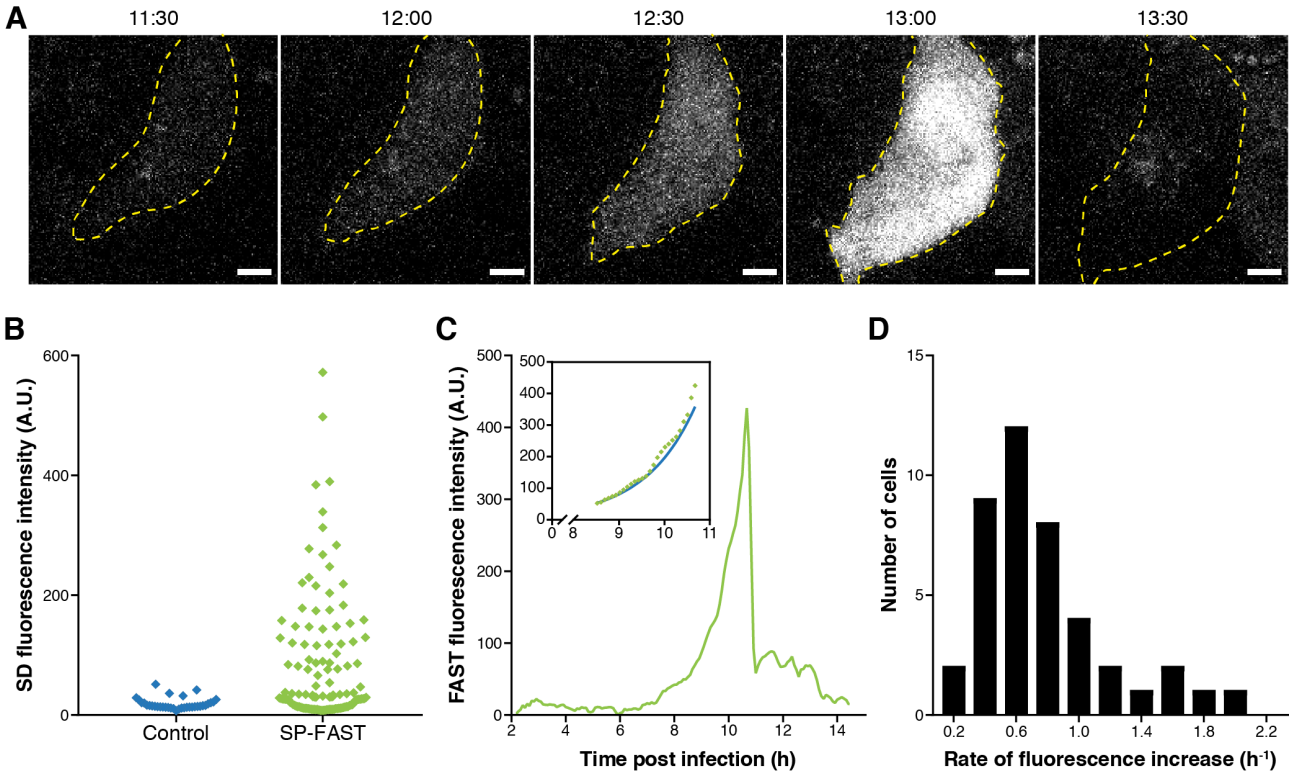


**Figure 2. Accumulation of secreted FAST in the cytoplasm of infected cells.**

(**A**) Spinning-disk fluorescence microscopy images of LoVo cells infected with *Lm* expressing SP-FAST at different time-points post-infection. The cell contours were segmented based on SiR-actin staining, and are indicated with a dashed yellow line. Scale bar, 5 µm.

(**B**) Dispersion of fluorescence intensities. Fluorescence emission at 562 nm (FAST:HBR-3,5-DM channel) was quantified over time within a region of fixed area in cells infected by *Lm* strains expressing either SP-FAST (in green, n=124) or mCherry as a negative control (in blue, n=35). As an indicator of the amplitude of fluorescence accumulation, the standard deviation of fluorescence intensity over time was plotted for each cell. A.U., arbitrary units.

(**C**) Intensity of FAST signals measured over time in a representative infected cell. Inset, exponential fit (in blue) obtained over the ascending part of the curve (in green dots).

(**D**) Distribution of the rates of increase of FAST fluorescence signals among the population of infected cells.

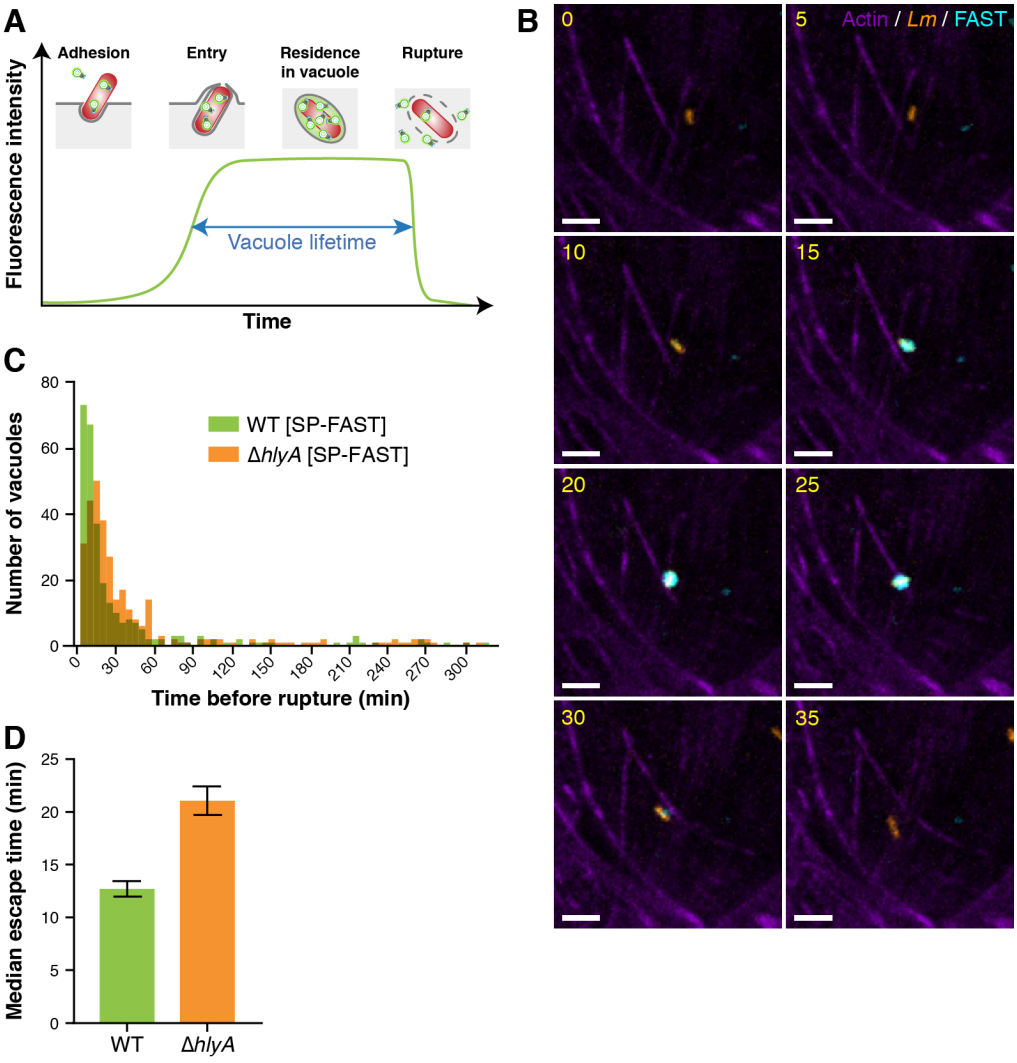


**Figure 3. Secreted FAST allows the tracking of *Listeria* entry vacuoles and the assessment of their lifetime.**

(**A**) Expected profile of fluorescence accumulation in internalisation vacuoles for *Lm* secreting SP-FAST. After bacterial adhesion, *Lm* enters epithelial cells via a zipper mechanism. Secreted FAST should start accumulating in vacuoles upon their closure, and then remain visible until vacuolar rupture. In each vacuole, a steady-state level of fluorescence might be temporarily reached, reflecting the equilibrium between bacterial secretion of FAST and its leakage in case of membrane permeation.

(**B**) Spinning-disk microscopy images of LoVo cells infected with *Lm ΔhlyA* expressing SP-FAST (cyan) and mCherry (orange) for 35 min after entry. The actin cytoskeleton (purple) was labelled with SiR-actin.

(**C**) Distribution of *Lm* residence times in internalisation vacuoles in LoVo cells. Green, WT strain carrying an integrated pPL2-SP-FAST plasmid (n=284); Orange, *ΔhlyA*::SP-FAST strain carrying an integrated pHpPL3-mCherry plasmid (n=306).

(**D**) Median half-lives of SP-FAST-labelled vacuoles calculated from the distribution displayed in (**C**).

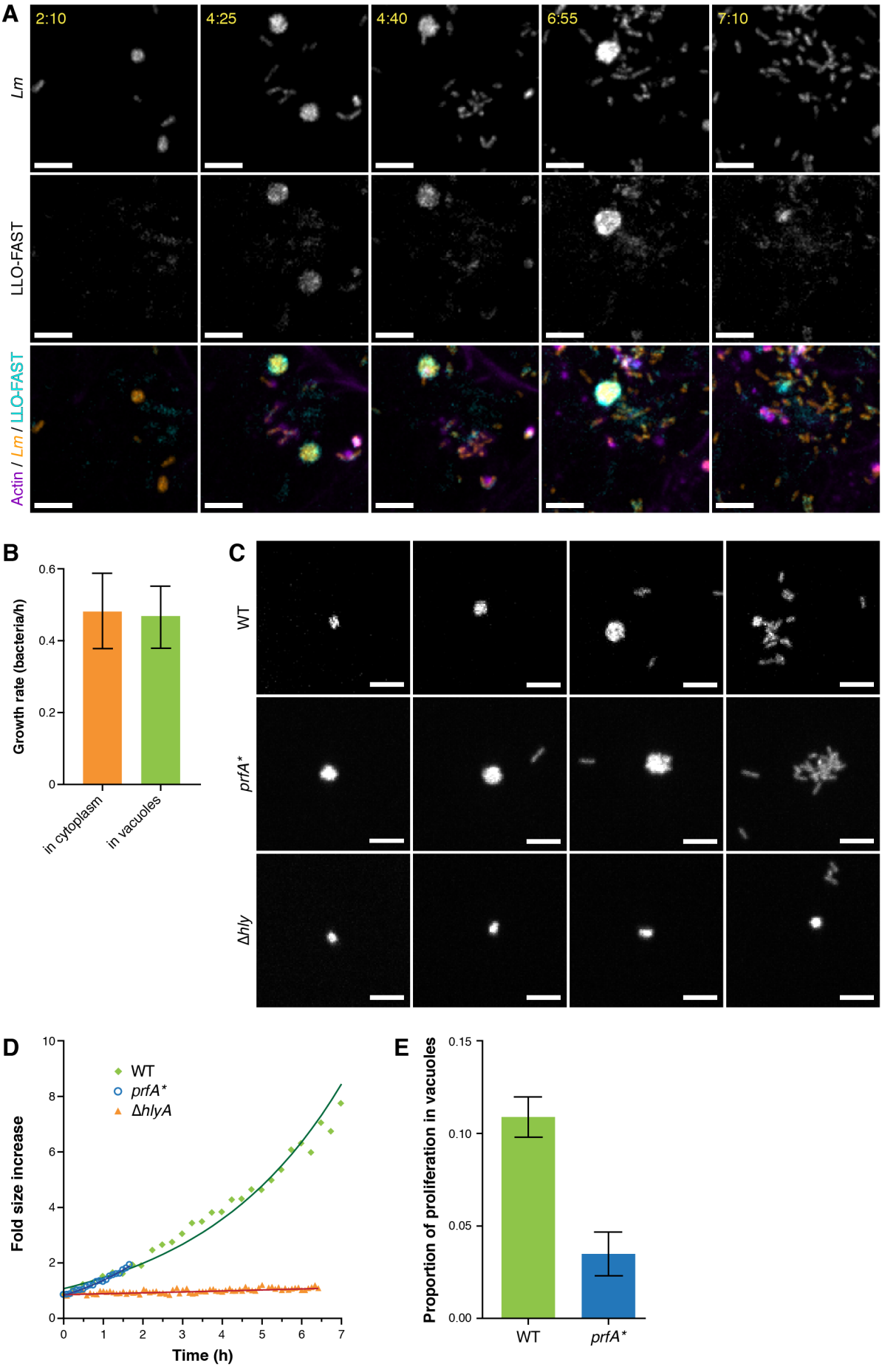

**Figure 4. *Listeria monocytogenes* can replicate inside long-term vacuoles decorated with LLO in epithelial cells.**

(**A**) Spinning-disk microscopy images of LoVo cells infected with *Lm* expressing both LLO-FAST (in cyan) and mCherry (in orange) at several time-points post-infection. SiR-actin staining is shown in purple. Scale bar, 5 µm.

(**B**) Growth rates of *Lm* expressing mCherry in the cytoplasm (orange, n=3) or in LRVs (green, n=7) in infected LoVo cells.

(**C**) Time-course of replication of mCherry-expressing *Lm* inside a LRV for the WT, the *prfA** and the Δ*hlyA* strains during the infection of LoVo cells. Scale bar, 5 µm.

(**D**) Quantification of the increase in volume of LRVs, and thus of the growth of the bacteria they contain, for the WT (green), the *prfA** (blue) or the Δ*hlyA* (orange) *Lm* strains in infected LoVo cells.

(**E**) Proportion of intracellular *Lm* that, starting from 2 h p.i., proliferated inside LVRs during the subsequent time-course of 12 h. Green, WT strain (n=193); blue, *prfA** strain (n=57).

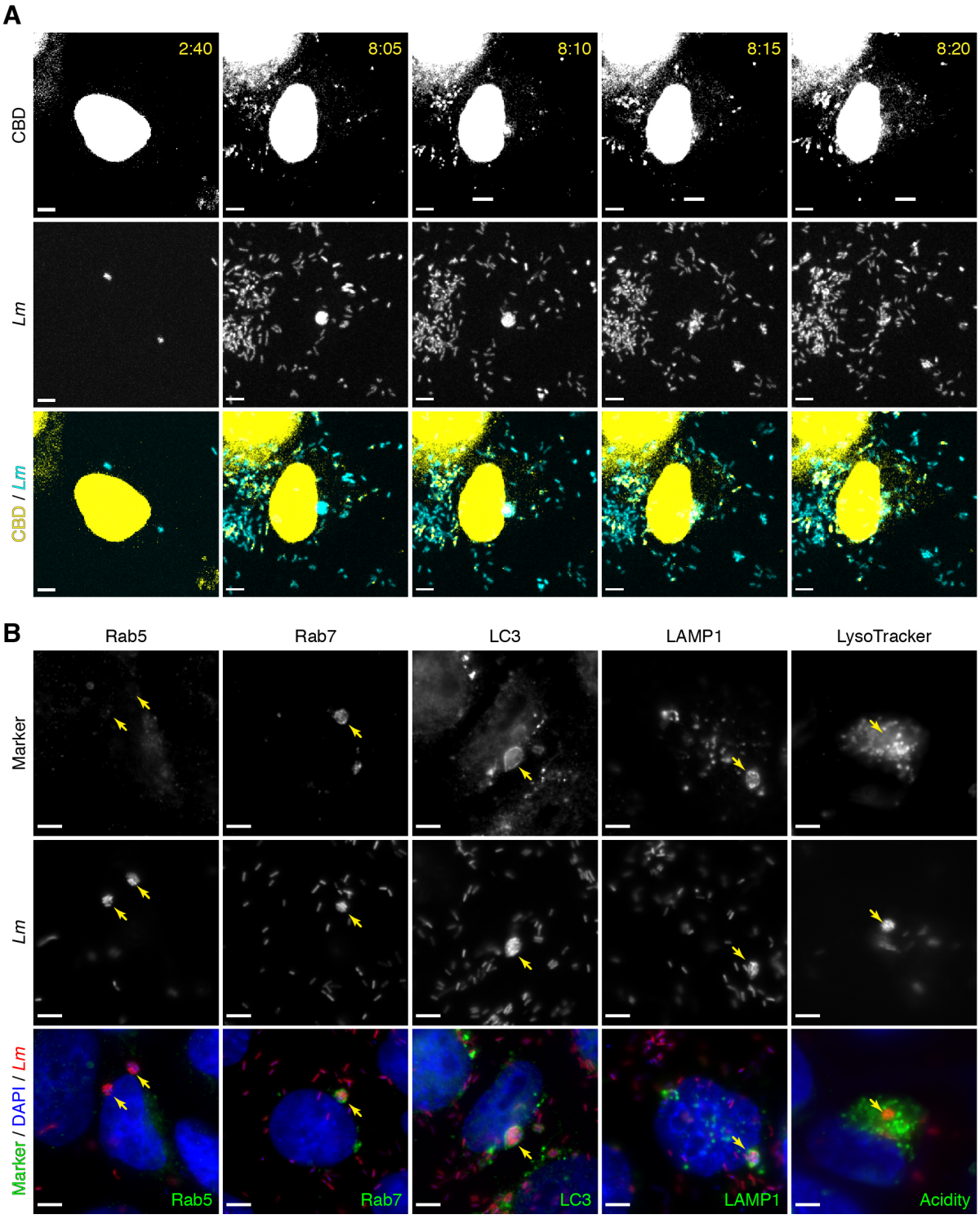


**Figure 5. *Listeria* epithelial LRVs originate from internalisation vacuoles and display typical markers of compartments deriving from LC3-associated phagocytosis.**

(**A**) Differential labelling by CBD-YFP of the cytosolic *versus* vacuolar populations of intracellular bacteria. LoVo cells were transfected with pEYFP-CBD (in yellow) 24 h before being infected with *Lm* expressing mCherry (in cyan), then imaged at different time-points post infection.

(**B**) Rab5, Rab7, LC3 and LAMP1 (in green) were detected by immunofluorescence in LoVo cells infected

for 3 h with mCherry-expressing bacteria (in red). For acidity staining, LoVo cells infected for 2 h with eGFP-expressing bacteria (in red) were stained with LysoTracker Deep Red (in green), and observed 1 h afterwards. Observations were performed on an inverted spinning disk microscope. Scale bars, 5 μm.

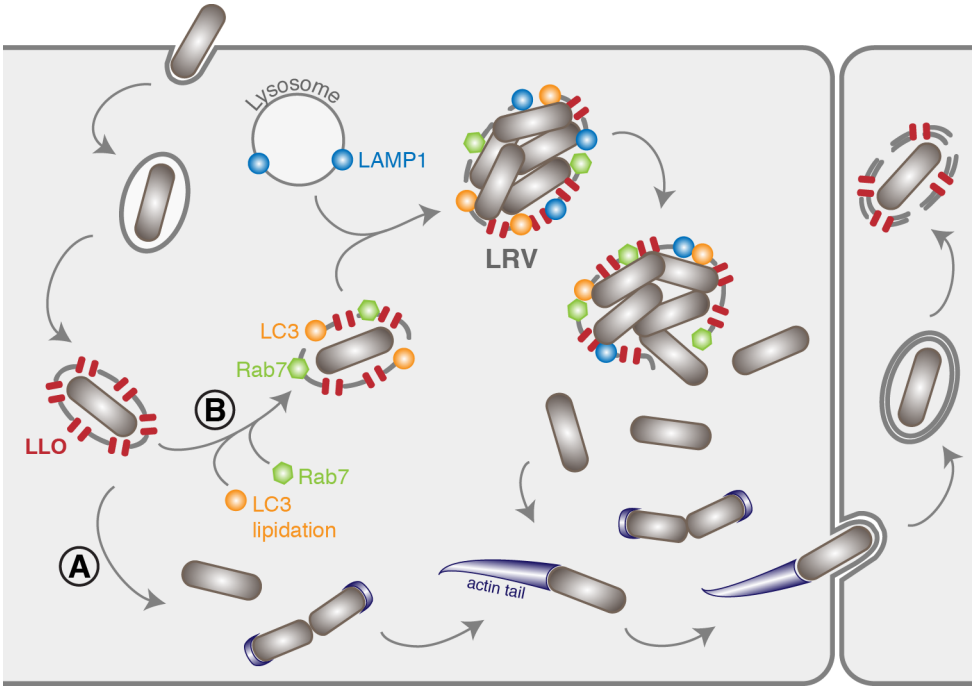


**Figure 6. Extended model of the intracellular life cycle of *Lm* in epithelial LoVo cells.**

(**A**) In the classical scenario, after receptor-mediated entry, *Lm* evades the vacuole thanks to the combined action of LLO and phospholipases.

(**B**) Here we identified a population of *Lm* that can remain for several hours and multiply inside LRVs. These compartments are neutral, positive for Rab7, LC3 and LAMP1, and permeated by LLO. This second population finally escapes into the cytoplasm at later time points.

# Movies

## Movie EV1. Accumulation of secreted FAST in the cytoplasm of infected cells.

LoVo cells infected with *Lm* expressing SP-FAST were observed between 2 and 14 h post-infection by spinning-disk microscopy. Scale bar, 10 µm.

## Movie EV2. Observation of secreted FAST signals in *Listeria* entry vacuoles.

LoVo cells infected with *Lm* expressing SP-FAST were observed between 0 and 3.25 h post-infection by spinning-disk microscopy. Green, FAST channel; red, mCherry channel; blue, SiR-actin channel. Tracks for individual internalisation vacuoles containing mCherry-bacteria and SP-FAST are displayed in yellow. Scale bar, 10 µm.

## Movie EV3. Background signals in the FAST channel when cells were infected with bacteria that do not secrete FAST.

LoVo cells infected with *Lm* expressing mCherry were observed between 0 and 3.25 h post-infection by spinning-disk microscopy. Acquisition parameters and contrasts were sets as in Mov. S2. Green, FAST channel (non-specific signals); red, mCherry channel; blue, SiR-actin channel. Scale bar, 10 µm.

## Movie EV4. Observation of the decoration of LRVs by LLO-FAST in *Listeria* cells infected by *Lm* LL195.

LoVo cells infected with *Lm* LL195 expressing both mCherry and LLO-FAST were observed between 2 and 8 h post-infection by spinning disk microscopy. Orange, FAST channel; cyan, mCherry channel; purple, SiR-actin channel. Scale bar, 5 µm.

## Movie EV5. Observation of the decoration of LRVs by LLO-FAST in *Listeria* cells infected by *Lm* EGD-e.

LoVo cells infected with *Lm* EGD-e expressing both mCherry and LLO-FAST were observed between 2 and 9 h post-infection by spinning disk microscopy. Orange, FAST channel; cyan, mCherry channel; purple, SiR-actin channel. Scale bar, 5 µm.

## Movie EV6. Imaging of the differential labelling by CBD-YFP of the cytosolic *versus* vacuolar populations of intracellular bacteria.

LoVo cells were transfected with pEYFP-CBD 24 h being infected with *Lm* expressing mCherry, then imaged by spinning disk microscopy from 2 to 8 h p.i. Yellow, CBD-YFP channel; cyan, mCherry channel. Scale bar, 5 µm.

# Expanded view figures

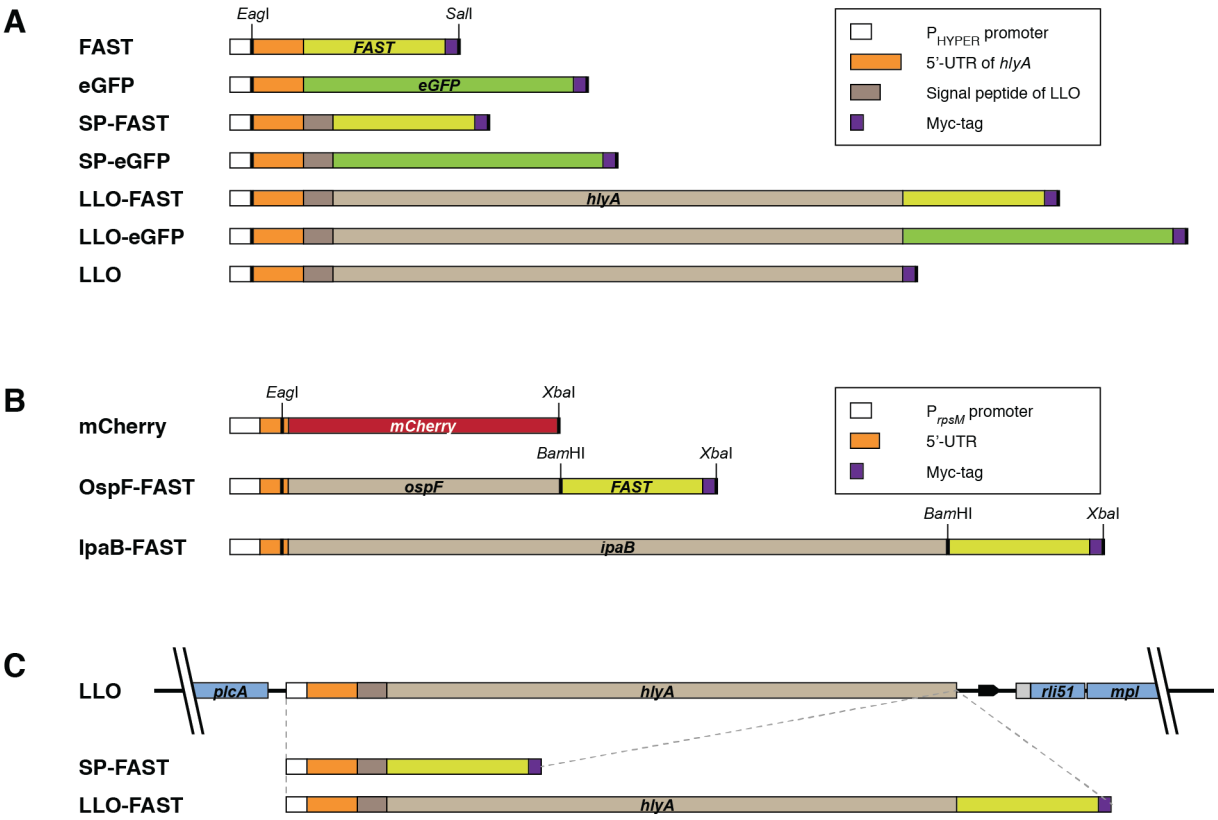


**Figure EV1. Diagram of constructs for *Listeria* and *Shigella* expression.**

(**A**) Constructs in the pAD vector derived from pPL2 (Lauer *et al*, 2002; Balestrino *et al*, 2010) for constitutive expression in *Listeria*.

(**B**) Constructs in the pSU2.1 vector for expression in *Shigella* (Campbell-Valois *et al*, 2015) (**C**) Constructs in the pMAD vector (Trieu-Cuot *et al*, 1991), for allelic replacements at the *hlyA* locus in *Listeria* genomes.

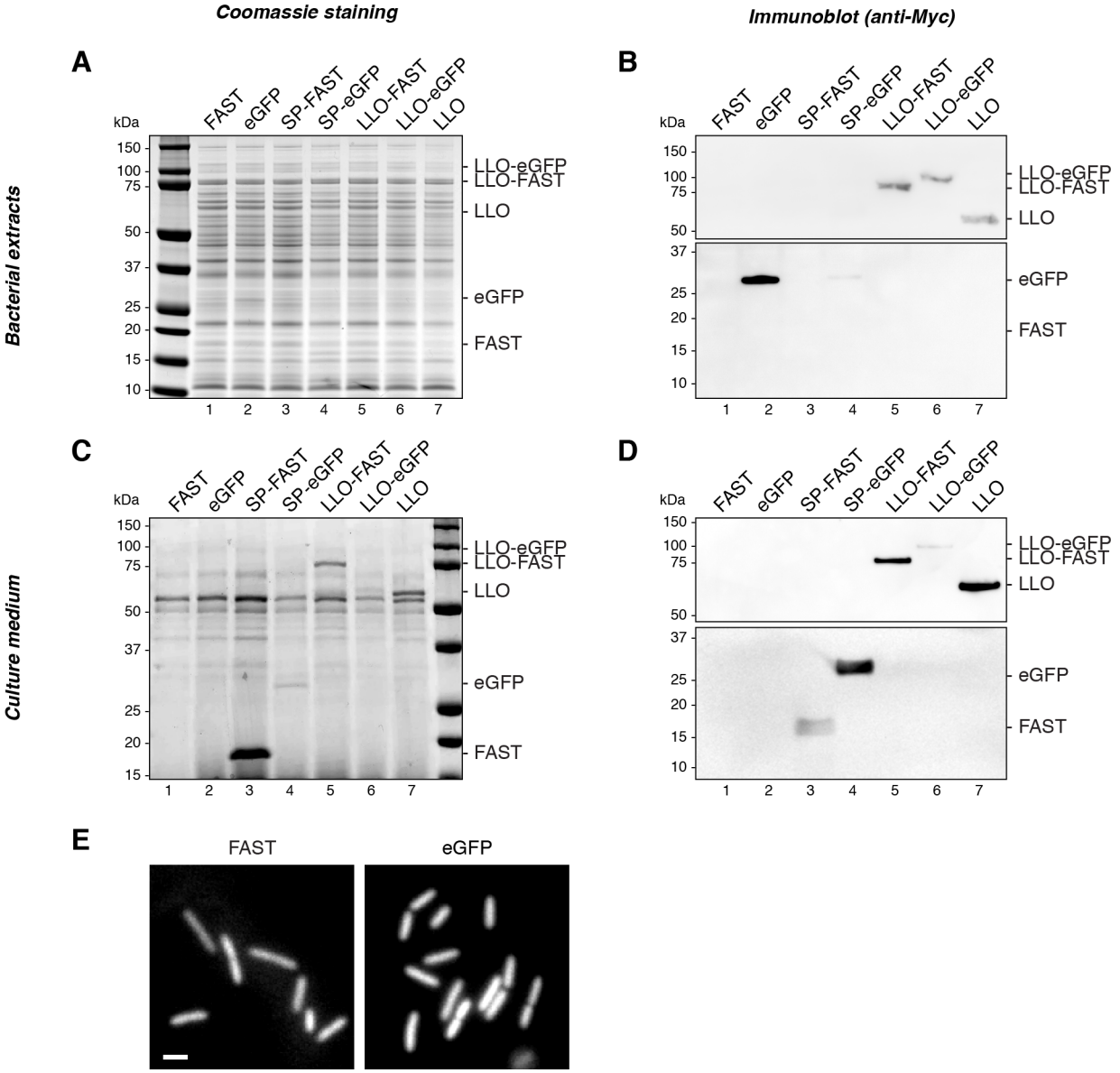


**Figure EV2. Production and secretion of the Myc-tagged fusion proteins by *Listeria monocytogenes* LL195 (constitutive expression from an integrated pAD vector).**

Protein production and secretion of Myc-tagged fusion proteins was assessed by colloidal Coomassie staining (**A**, **C**) and immunoblotting with anti-Myc antibodies (**B**, **D**) of bacterial total extracts (**A**, **B**) and culture supernatant fractions (**C**, **D**) from overnight-grown cultures in BHI, separated by SDS-PAGE. (**E**) Epifluorescence microscopy observation of strains producing non-secreted FAST or eGFP. Scale bar, 2 µm.

Most Myc-tagged protein constructs were detected by immunoblotting in the corresponding bacterial pellet fraction, indicating that transgenes were expressed, even though in varying amounts (**B**, lanes 2, 4-7). Constructs harbouring the LLO SP or full-length LLO were recovered in bacterial supernatants (**C**, **D**, lanes 3-7), suggesting that the SP of LLO promoted Sec-dependent export of not only of FAST or FAST-tagged proteins, but also of eGFP-fusion proteins. The secretion of eGFP-tagged proteins seemed less efficient than that of FAST-tagged protein (**C**, compare lane 3 with 4; **D**, compare lane 5 with 6), consistent with previous

reports that eGFP is a poor substrate for Sec-dependent secretion (Dammeyer & Tinnefeld, 2012). Constructs devoid of signal peptides were not detected in supernatant fractions (**C**, **D**, lanes 1-2), arguing against the release of proteins into the culture medium due to bacterial lysis.

For technical reasons likely due to the small size of FAST-Myc (15 kDa), it was not or barely detected by immunoblotting (**B**, **D**, lanes 1, 3); nevertheless, a strong signal corresponding to this polypeptide was visible on Coomassie-stained gels of the supernatant fractions, attesting of its secretion (**C**, lane 3). For bacterial pellet fractions (**A**, lanes 1, 3), signal from other proteins masked possible bands from that polypeptide; however, observation in microscopy (**E**) confirmed the non-secreted form of FAST was also produced.

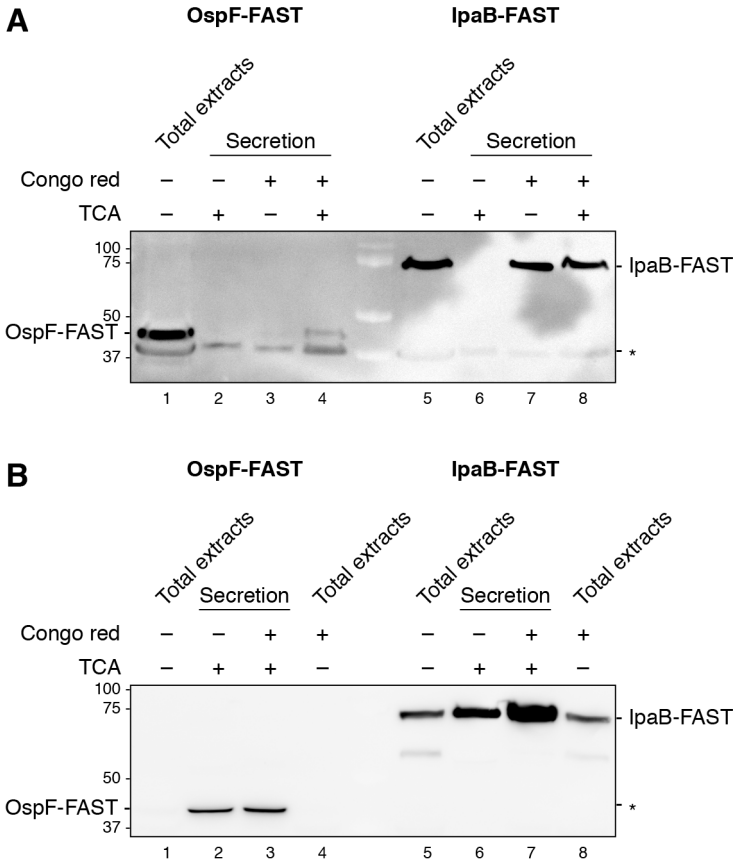


**Figure EV3. Production and secretion of the Myc-tagged fusion proteins by *Shigella flexneri* M90T (constitutive expression from a pSU2.1rp vector).**

Protein production and secretion of Myc-tagged fusion proteins was assessed by immunoblotting with anti-Myc antibodies of bacterial total extracts culture supernatant fractions, with or without induction of secretion by the T3SS using Congo red, and with or without TCA precipitation in order to concentrate samples. (**A**) Samples from wild type M90T *Shigella flexneri*. (**B**) Samples from M90T Δ*ipaD*, in which T3SS secretion is constitutive. *, non-specific band.

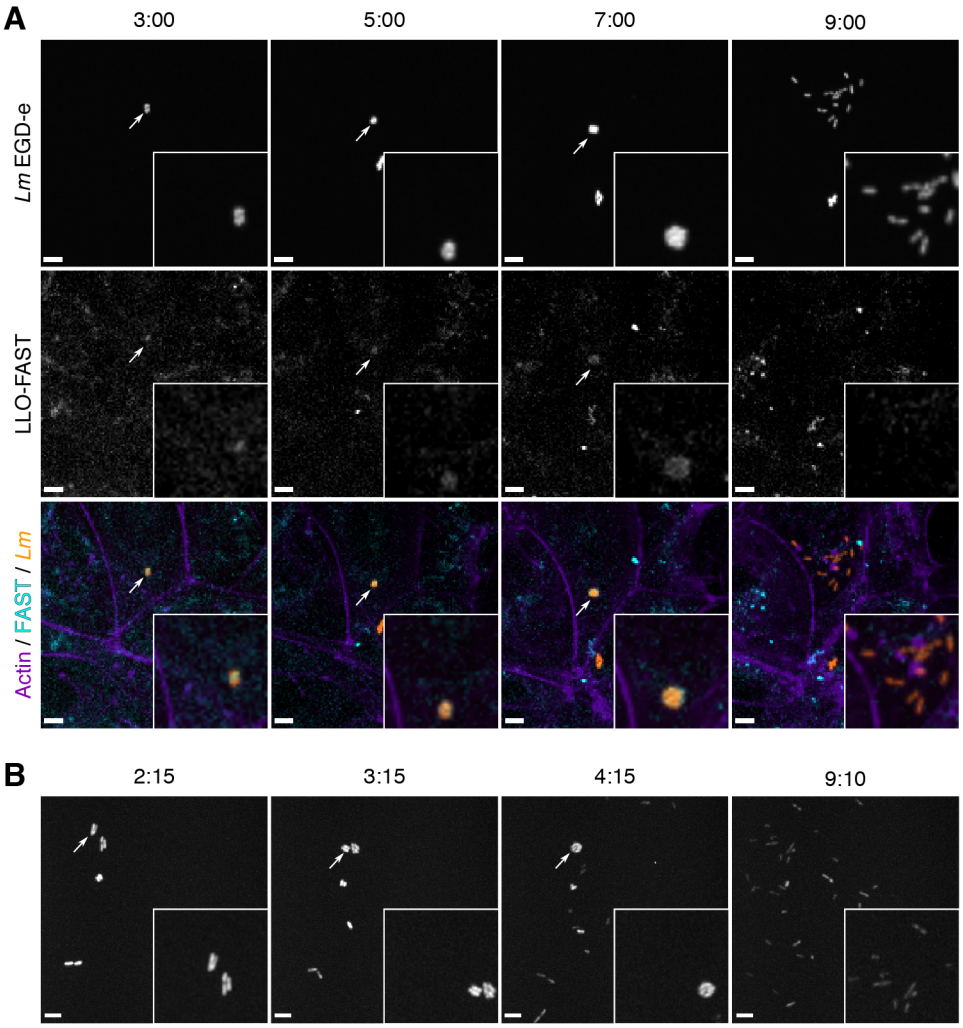


**Figure EV4. Proliferation of *Lm* inside LRVs is also observed when using the EGD-e strain in LoVo cells, or the LL195 strain in Caco-2 cells.**

(**A**) LoVo cells infected with *Lm* EGD-e expressing both mCherry and LLO-FAST were observed between 2 and 8 h post-infection by spinning disk microscopy. On the merged image, LLO-FAST is in cyan, mCherry is in orange, and SiR-actin is in purple. Scale bar, 5 µm.

(**B**) Time-course of replication of mCherry-expressing *Lm* LL195 inside a LRV, observed in the Caco-2 cell line. Scale bar, 5 µm.

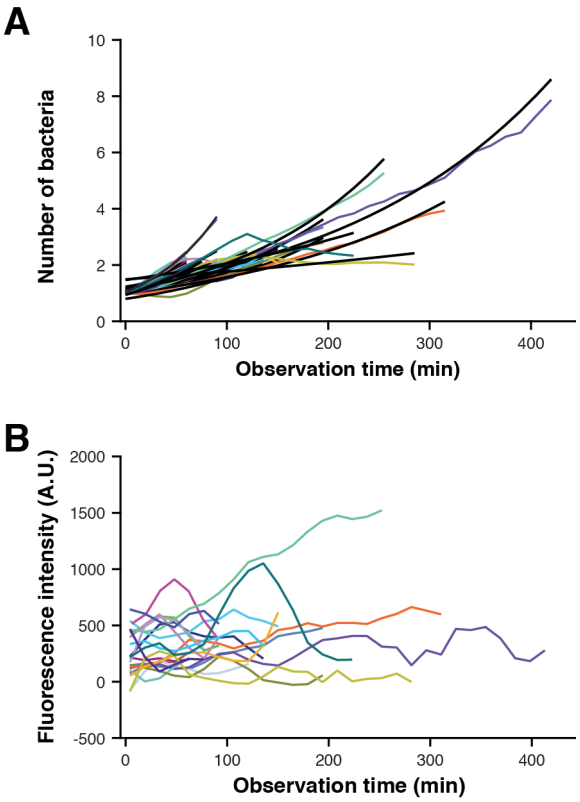


**Figure EV5. Number of bacteria and fluorescence of LLO-FAST inside LRVs over time.**

LoVo cells were infected with *Lm* carrying an integrated pHpPL3-mCherry plasmid, that allowed their segmentation and the counting of the number of bacteria per LRV over time (**A**). These bacteria were also C-terminally tagged with FAST at the *hlyA* locus. The quantification of the fluorescence over time in the FAST channel (**B**) is therefore reporting for the concentration of LLO-FAST in LRVs.

# Appendix

## Table of contents of the Appendix

Appendix figures S1 to S4

Appendix tables S1 to S2

## Appendix figures

**A** **gfAL001 – *Eag*I-5'-UTR$_{hlyA}$-SP$_{hlyA}$-FAST$_{Listeria}$-Myc-STOP-*Sal*I**

tgtgt***CGGCCG***ataaagcaagcatataatattgcgtttcatctttagaag
cgaatttcgccaatattataattatcaaaagagaggggtggcaaacggta
tttggcattattaggttaaaaaatgtagaaggagagtgaaaccc**ATG**AAA
AAAATAATGCTAGTTTTTATTACACTTATATTAGTTAGTCTACCAATTGC
GCAACAAACTGAAGCAAAGGATGAACATGTTGCTTTCGGTTCTGAAGATA
TCGAAAATACACTTGCAAAAATGGATGATGGTCAACTTGATGGCCTAGCA
TTCGGTGCTATTCAACTTGACGGCGACGGCAACATTCTTCAATACAACGC
GGCAGAAGGAGATATTACTGGTCGTGATCCAAAACAAGTAATTGGAAAAA
ACTTTTTCAAAGACGTTGCTCCAGGGACCGATAGCCCTGAATTCTATGGA
AAATTTAAAGAAGGTGTAGCTTCTGGCAATCTAAACACTATGTTCGAATG
GATGATCCCAACATCACGTGGACCAACAAAAGTTAAAGTTCATATGAAAA
AAGCACTAAGCGGAGATTCATATTGGGTTTTTGTTAAACGTGTAgaacaa
aaacttatcagcgaagaagatttaTAA***GTCGAC***ctcgagggggggcccGG
TACCagctt

**B** **gfAL002 – *Bam*HI-FAST$_{Shigella}$-Myc-STOP-*Xba*I**

ATG***ggatcc***GAACATGTTGCGTTCGGCAGCGAAGATATTGAGAACACCTT
AGCTAAAATGGACGATGGTCAGTTAGACGGCCTGGCTTTTGGTGCGATCC
AGCTGGACGGCGACGGCAACATCCTGCAGTACAACGCGGCTGAAGGTGAT
ATCACCGGTCGCGATCCGAAACAGGTGATCGGCAAAAACTTCTTCAAAGA
CGTTGCGCCGGGTACTGACTCTCCGGAATTCTACGGTAAATTTAAAGAGG
GTGTCGCGTCCGGTAACCTGAACACCATGTTCGAATGGATGATCCCAACC
TCCCGCGGCCCAACCAAAGTTAAAGTCCACATGAAAAAAGCACTGAGCGG
CGATTCTTATTGGGTGTTCGTTAAACGTGTTgaacagaaactgatctctg
aggaagatctgTAA***tctaga***gtcg

**Appendix figure S1. Synthetic gene fragments with codon-optimized sequences for expression in *Listeria* (A) or *Shigella* (B).**

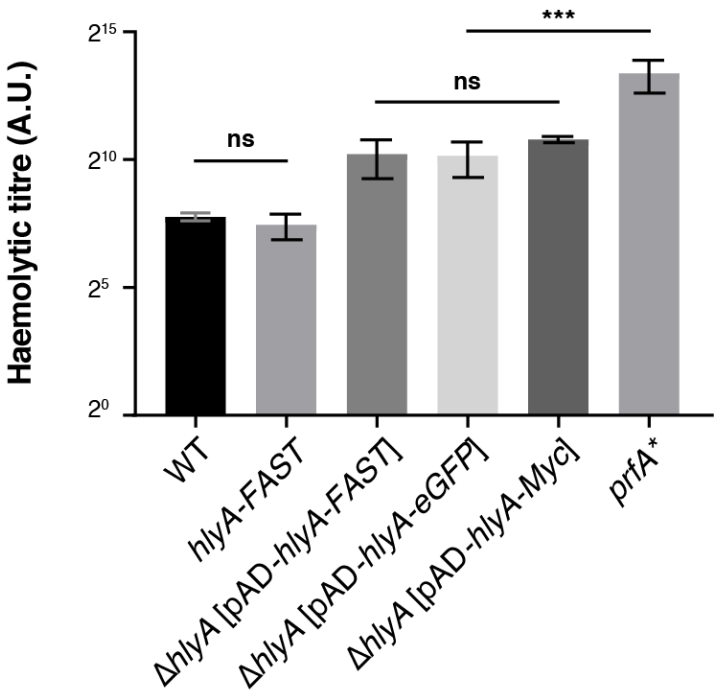


**Appendix figure S2. Haemolytic properties of the *Listeria monocytogenes* strains producing FAST– or eGFP–tagged fusion LLO used in this study.**

The haemolytic titre measured for the strain where LLO was C-terminally tagged with FAST-Myc at the *hlyA* locus (*hlyA-FAST*) did not differ from that of the WT *Lm* strain. Haemolytic titres were enhanced for *ΔhlyA* deletion strains that had been complemented by *hlyA* fusion genes under control of the strong, constitutive $P_{HYPER}$ promoter in the pAD vector. Fusion with FAST-Myc or eGFP-Myc did not affect haemolytic properties, compared to a simple fusion with Myc. None of these strains reached the intense haemolytic properties of the *prfA** strain, where the expression of *Lm* virulence genes (including *hlyA*) is deregulated, due to the constitutive activity of the transcriptional activator PrfA (Ripio *et al*, 1997). The haemolytic titre of the *ΔhlyA* strain being null, it was not represented on this graph. ANOVA was used for statistical testing. ns, non-significant; ***, $p < 0.001$.

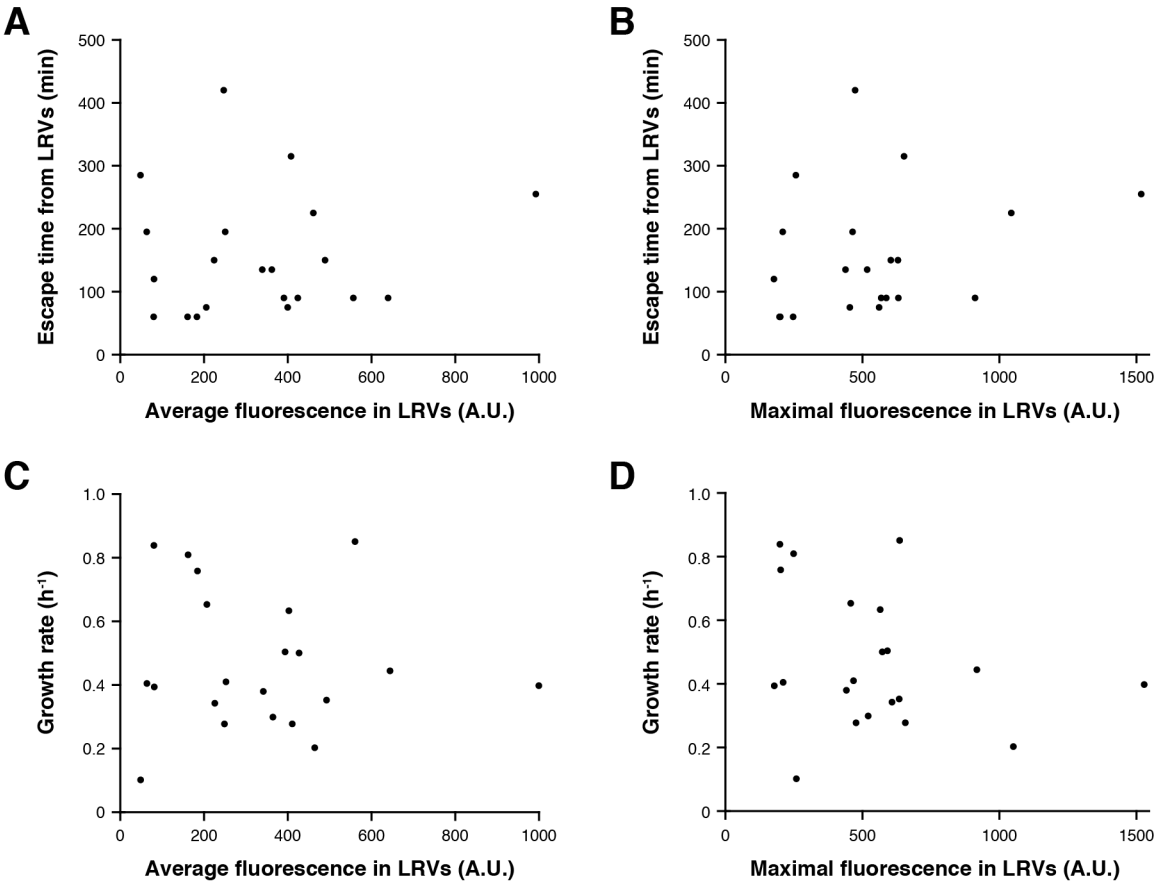


**Appendix figure S3. Correlation between the fluorescence generated by LLO-FAST in LRVs and either the time of bacterial escape from, or the growth rate in, these compartments.**

From the same images as the ones analysed in Fig EV5, the average intensity of fluorescence generated by the secretion of LLO-FAST (**A, C**) and the maximum intensity of LLO-FAST fluorescence (**B, D**) were extracted for each LRV (n = 21), and correlated with the duration of this compartment from the beginning of acquisition until membrane rupture (**A, B**) or with the growth rate of bacteria in this compartment, defined by the rate of increase of the size of the mCherry-labelled volume occupied by intravacuolar bacteria (**C, D**).

# Appendix tables

## Appendix table S1. Bacterial strains

| Strain | Description | Resistance | Reference |
|---|---|---|---|
| **LL195** | *L. monocytogenes* LL195 | | (Weinmaier *et al*, 2013) |
| **BUG1600** | *L. monocytogenes* EGD-e | | (Glaser *et al*, 2001) |
| **BUG2479** | *E. coli* DH5α [pAD-*cGFP*] | Cm 35 | (Balestrino *et al*, 2010) |
| **AG87** | *E. coli* Rosetta(DE3)pLysS [pET28a-*FAST*] | | (Plamont *et al*, 2016) |
| **FXCV1** | *E. coli* DH5α [pSU2.1rp-*mCherry*] | Cm 35 | (Campbell-Valois *et al*, 2015) |
| **JDS1** | *E. coli* SM10 [pHpPL3-*mCherry*] | | (Vincent *et al*, 2016) |
| **M90T** | *S. flexneri* M90T | | (Sansonetti *et al*, 1982) |
| **SF622** | *S. flexneri* M90T Δ*ipaD* | Km 50 | (Ménard *et al*, 1993) |
| **BIRD8** | *E. coli* NEB5α [pAD-*SP-FAST-Myc*]‡ | Cm 35 | This work |
| **BIRD9** | *E. coli* NEB5α [pAD-*hlyA-Myc*] | Cm 35 | This work |
| **BIRD13** | *L. monocytogenes* LL195 [pAD-*SP-FAST-Myc*] | Cm 7 | This work |
| **BIRD14** | *L. monocytogenes* LL195 [pAD-*hlyA-Myc*] | Cm 7 | This work |
| **BIRD15** | *E. coli* NEB5α [pAD-*FAST*] | Cm 35 | This work |
| **BIRD16** | *L. monocytogenes* LL195 [pAD-*FAST-Myc*] | Cm 7 | This work |
| **BIRD17** | *E. coli* NEB5α [pAD-*eGFP-Myc*] | Cm 35 | This work |
| **BIRD18** | *L. monocytogenes* LL195 [pAD-*eGFP-Myc*] | Cm 7 | This work |
| **BIRD19** | *E. coli* NEB5α [pAD-*SP-eGFP-Myc*] | Cm 35 | This work |
| **BIRD20** | *L. monocytogenes* LL195 [pAD-*SP-eGFP-Myc*] | Cm 7 | This work |
| **BIRD32** | *E. coli* NEB5α [pAD-*hlyA-FAST-Myc*] | Cm 35 | This work |
| **BIRD33** | *E. coli* NEB5α [pAD-*hlyA-eGFP-Myc*] | Cm 35 | This work |
| **BIRD38** | *L. monocytogenes* LL195 [pAD-*hlyA*-FAST-Myc] | Cm 7 | This work |
| **BIRD39** | *L. monocytogenes* LL195 [pAD-*hlyA*-eGFP-Myc] | Cm 7 | This work |
| **BIRD62** | *E. coli* NEB5α [pSU2.1rp-*ospF-FAST-Myc*] | Cm 35 | This work |
| **BIRD64** | *E. coli* NEB5α [pSU2.1rp-*ipaB-FAST-Myc*] | Cm 35 | This work |
| **BIRD62** | *E. coli* NEB5α [pSU2.1rp-*ospF-FAST-Myc*] | Cm 35 | This work |
| **BIRD64** | *E. coli* NEB5α [pSU2.1rp-*ipaB-FAST-Myc*] | Cm 35 | This work |
| **BIRD66** | *S. flexneri* M90T [pSU2.1rp-*ospF-FAST-Myc*] | Cm 20 | This work |
| **BIRD67** | *S. flexneri* M90T [pSU2.1rp-*ipaB-FAST-Myc*] | Cm 20 | This work |
| **BIRD84** | *S. flexneri* M90T Δ*ipaD* [pSU2.1rp-*ospF-FAST-Myc*] | Km 50, Cm 15 | This work |
| **BIRD85** | *S. flexneri M90T* Δ*ipaD* [pSU2.1rp-*ipaB-FAST-Myc*] | Km 50, Cm 15 | This work |
| **BIRD127** | *L. monocytogenes* LL195 Δ*hlyA* | | This work |
| **BIRD204** | *E. coli* NEB5α [pMAD-*hlyA-FAST-Myc*] | Ap 100 | This work |
| **BIRD207** | *L. monocytogenes* EGD-e *hlyA-FAST-Myc* | | This work |
| **BIRD213** | *E. coli* NEB5α [pMAD-Δ*hlyA*::*SP-FAST-Myc*] | Ap 100 | This work |
| **BIRD217** | *L. monocytogenes* LL195 [pHpPL3-*mCherry*] | Cm 7 | This work |
| **BIRD220** | *L. monocytogenes* EGD-e *hlyA-FAST-Myc* [pHpPL3-*mCherry*] | Cm 7 | This work |

| | | | |
|---|---|---|---|
| **BIRD234** | *L. monocytogenes* LL195 *prfA** | | This work |
| **BIRD240** | *L. monocytogenes* LL195 *hlyA-FAST-Myc* | | This work |
| **BIRD244** | *L. monocytogenes* LL195 *hlyA-FAST-Myc* [pHpPL3-*mCherry*] | Cm 7 | This work |
| **BIRD250** | *L. monocytogenes* LL195 Δ*hlyA* [pHpPL3-*mCherry*] | Cm 7 | This work |
| **BIRD251** | *L. monocytogenes* LL195 *prfA** [pHpPL3-*mCherry*] | Cm 7 | This work |
| **BIRD252** | *L. monocytogenes* LL195 Δ*hlyA*::*SP-FAST-Myc* [pHpPL3-*mCherry*] | Cm 7 | This work |
| **BIRD256** | *L. monocytogenes* LL195 Δ*hlyA* [pAD-*FAST-Myc*] | Cm 7 | This work |
| **BIRD257** | *L. monocytogenes* LL195 Δ*hlyA* [pAD-*SP-FAST-Myc*] | Cm 7 | This work |
| **BIRD258** | *L. monocytogenes* LL195 Δ*hlyA* [pAD-*hlyA-FAST-Myc*] | Cm 7 | This work |
| **BIRD259** | *L. monocytogenes* LL195 Δ*hlyA* [pAD-*eGFP-Myc*] | Cm 7 | This work |
| **BIRD260** | *L. monocytogenes* LL195 Δ*hlyA* [pAD-*SP-eGFP-Myc*] | Cm 7 | This work |
| **BIRD261** | *L. monocytogenes* LL195 Δ*hlyA* [pAD-*hlyA-eGFP-Myc*] | Cm 7 | This work |
| **BIRD262** | *L. monocytogenes* LL195 Δ*hlyA* [pAD-*hlyA-Myc*] | Cm 7 | This work |

‡ All pAD constructs contain the $P_{HYPER}$ constitutive promoter, the 5'-UTR of the *hlyA* gene, and the desired fusion protein. To simplify reading, the C-terminal Myc tag of constructs is not included in the plasmid names in the main text of the article. Concentartions of antibiotics are given in μg/ml. Cm, chloramphenicol; Ap, ampicillin; Km, kanamycin.

## Appendix table S2. Oligonucleotides

| Name | Description | Sequence | Ref. |
|---|---|---|---|
| **oAL543** | *Eag*I-UTR$_{hlyA}$ fw | tgtgtCGGCCGataaagcaa | This work |
| **oAL544** | *Xho*I-*Sal*I-Myc rv | CCctcgagGTCGACTTAtaa | This work |
| **oAL545** | FAST-UTR$_{hlyA}$ rv* | acatgttcCATGGGTTTCACTCTCCTTC | This work |
| **oAL546** | UTR$_{hlyA}$-FAST fw | tgaaacccATGGAACATGTTGCTTTCGG | This work |
| **oAL547** | Myc-GFP rv | atttttgttcTTTGTATAGTTCATCCATGCC | This work |
| **oAL548** | GFP-Myc fw | actatacaaaGAACAAAAATTAATCTCTGAA | This work |
| **oAL549** | *Eag*I-UTR$_{hlyA}$ fw | gtgtgtCGGCCGataaagcaagcatataatattgcg | This work |
| **oAL550b** | *Sal*I-Myc-LLO rv | cgagGTCGACTTAtaaatcttcttcagagattaatttttgTTCGAT TGGATTATCTACTT | This work |
| **oAL551b** | FAST-LLO rv | gcaacaTGTTCGATTGGATTATCTACTTTAT | This work |
| **oAL552b** | LLO-FAST fw | ataatccaatcGAACATGTTGCTTTCGGTTC | This work |
| **oAL553** | GFP-SP$_{hlyA}$ rv‡ | ctcctttactATCCTTTGCTTCAGTTTGTTG | This work |
| **oAL554** | SP$_{hlyA}$-GFP fw | gcaaaggatAGTAAAGGAGAAGAACTTTTC | This work |
| **oAL651** | LLO-GFP rv | TCTCCTTTACTatgttcGATTGGATTATCTAC | This work |
| **oAL652** | GFP-LLO fw | CAATCgaacatAGTAAAGGAGAAGAACTTTTC | This work |
| **oAL703** | *Kpn*I-*ipaB* fw | ctcGGTACCaaggagtaattattATGCAT | This work |
| **oAL704** | *Bam*HI-*ipaB* rv | CATGTTCggatccAGCAGTAGTTTGTTGCAAAAT | This work |
| **oAL705** | OspF-*Bam*HI-FAST fw | GATAGAGggatccGAACATGTTGCGTTCGGCAG | This work |
| **oAL706** | *Xba*I-Myc rv | cgactctagaTTAcagatcttcctcagaga | This work |
| **oAL707** | *Kpn*I-OspF fw | ctcGGTACCagaggacgttttctATGCCC | This work |
| **oAL708** | *Bam*HI-OspF rv | TTCggatccCTCTATCATCAAACGATAAAAT | This work |
| **oAL974** | *Sal*I-*hlyA* fw | TCCATATGACgtcgacAGCATTTAAAGCTGTA | This work |
| **oAL975** | 3' of *hlyA*-Myc rv | ttacttttacaaTTAtaaatcttcttcgctga | This work |
| **oAL976** | Myc-3' of *hlyA* fw | gaagatttaTAAttgtaaaagtaataaaaaattaag | This work |
| **oAL977** | *Bgl*II-*mpl* rv | TTAACTAGACagatctTTGTGGGTATCAGC | This work |
| **oAL981** | *Sal*I-*plcA* fw | TCCATATGACgtcgacACTCGGACCATTGTAG | This work |
| **oAL984** | FAST-SP$_{hlyA}$ rv | aaagcaacatgttcATCCTTTGCTTCAGTTTG | This work |
| **oAL985** | SP$_{hlyA}$-FAST fw | ggatGAACATGTTGCTTTCG | This work |

* UTR$_{hlyA}$ refers to the 5'-UTR of the *hlyA* gene, bringing a ribosome binding site (RBS) and used to enhance gene expression (Shen & Higgins, 2005). ‡ SP$_{hlyA}$ indicates to the sequence encoding the signal peptide from LLO (*hlyA* gene). Fw, forward strand; rv, reverse strand.